Carbazole-based Eu^{3+} complexes for two-photon microscopy imaging of live cells

Ji-Hyung Choi, Adam Nhari, Thibault Charnay, Baptiste Chartier, Lucile Bridou, Guillaume Micouin, Olivier Maury, Akos Banyasz, Sule Erbek, Alexei Grichine, et al.

Carbazole-based Eu^{3+} complexes for two-photon microscopy imaging of live cells

Ji-Hyung Choi,[a] Adam Nhari,[a,b] Thibault Charnay,[ab] Baptiste Chartier,[ab] Lucile Bridou,[c] Guillaume Micouin,[c] Olivier Maury,[c] Akos Banyasz,[c] Sule Erbek,[d,e] Alexei Grichine,[d] Véronique Martel-Frachet,[d,e] Fabrice Thomas,[b] Jennifer K. Molloy,[b] and Olivier Sénèque*[a]

[a] Univ. Grenoble Alpes, CNRS, CEA, IRIG, LCBM (UMR 5249), F-38000 Grenoble, France.

[b] Univ. Grenoble Alpes, CNRS, DCM (UMR 5250) F-38000 Grenoble, France.

[c] CNRS, ENS de Lyon, LCH, UMR 5182, F-69342 Lyon, France.

[d] Univ. Grenoble Alpes, INSERM U1209, CNRS UMR 5309, Institute for Advanced Biosciences, F-38000 Grenoble, France.

[e] EPHE, PSL Research University, 4-14 rue Ferrus, 75014 Paris, France

Email: *olivier.seneque@cea.fr*

Abstract

Lanthanide(III) complexes with two-photon absorbing antennas are attractive for microscopy imaging of live cells because they can be excited in the NIR. We describe the synthesis and the luminescence and imaging properties of two Eu^{3+} complexes, **mTAT[Eu·L-CC-Ar-Cz]** and **mTAT[Eu·L-Ar-Cz]**, with (*N*-carbazolyl)-aryl-alkynyl-picolinamide and (*N*-carbazolyl)-aryl-picolinamide antennas, respectively, conjugated to the TAT cell penetrating peptides. Contrary to what was previously observed with related Eu^{3+} complexes with carbazole-based antennas in mixture of water and organic solvents, these two complexes show very low emission quantum yield (Φ_{Eu} < 0.002) in purely aqueous buffers. A detailed spectroscopic study of on **mTAT[Eu·L-Ar-Cz]** reveals that the quantum yield of emission is strongly polarity-dependent – the less polar the medium, the higher the quantum yield – and that the emission quenching in water is likely due to a photoinduced electron transfer between the excited carbazole-based antenna and Eu^{3+} that efficiently competes with the energy transfer process. Nevertheless, **mTAT[Eu·L-Ar-Cz]** shows a significant two-photon cross-section of 100 GM at 750 nm, which is interesting for two-photon microscopy. The live cell imaging properties of **mTAT[Eu·L-Ar-Cz]** and two other conjugates were investigated. Cytosolic delivery was clearly evidenced in the case of **mTAT[Eu·L-Ar-Cz]** when cells are co-incubated with this compound and a non-luminescent dimeric TAT derivative, dFFLIPTAT.

Keywords

Peptide – Lanthanide – Carbazole – Luminescence – Microscopy

Introduction

Trivalent lanthanide cations (Ln^{3+}) have desirable luminescence properties for biological imaging.[1–10] Their emission spectra display sharp lines at fixed wavelengths, independent of the environment, that constitutes a fingerprint of each Ln.[11] Depending on the Ln^{3+}, the emission spans the UV-visible-NIR range, with Tb^{3+}, Eu^{3+}, Dy^{3+} and Sm^{3+} emitting in the visible and Dy^{3+}, Sm^{3+}, Nd^{3+}, Yb^{3+} et Er^{3+} emitting in the NIR for the most emissive Ln^{3+}. Additionally, luminescence lifetimes of Ln^{3+} are much longer (micro to millisecond range) than those of the biological, *i.e.* organic or endogenous, fluorescence (nanosecond range), allowing suppression of the biological background by time-gated detection experiments or easy discrimination between Ln^{3+} emission and biological background emission by lifetime measurements.[12] Due to the low extinction coefficient of direct Ln^{3+} absorption (< 5 M^{-1} cm^{-1}), efficient sensitization of Ln^{3+} luminescence relies on the antenna effect, *i.e.* on the use of a proximal light-harvesting organic chromophore that can transfer energy to the Ln^{3+} to efficiently populate its emitting excited state (Figure 1).[13] However, Tb^{3+} and Eu^{3+}, the most performant Ln^{3+} emitters in the visible, require antennas that absorb in the UV that is damaging for cells. This drawback can be circumvented by using two-photon (2P) absorbing antennas. 2P absorption corresponds to the simultaneous absorption of two photons of half the energy required by one photon absorption. 2P absorbing antennae make lanthanide complexes attractive for cell imaging using 2P microscopy (2PM)[14] with red-NIR excitation above 700 nm.[15–21] Like laser scanning confocal microscopy, 2P microscopy allows imaging of a cell section benefiting from an excitation localized in a small volume corresponding to the focal point of the laser. Regarding photophysical properties, the most interesting complexes for cell imaging are those featuring a poly-aza-macrocycle (tacn, cyclen, pyclen) with pendant picolinate push-pull antennae coordinating the Ln^{3+}.[17,22–27] Best 2P absorbing antennae for Tb^{3+}/Dy^{3+}, Eu^{3+}/Sm^{3+} and Yb^{3+} were alkoxy-aryl-, alkoxy-aryl-alkynyl- and dialkyamino-aryl-alkynyl-picolinate ones, respectively. However, most of these complexes fail to enter live cells and the intracellular probe imaging required cell fixation and membrane permeabilization, that had to be done before incubating cells with the probe. As a consequence, only dead cells are imaged. Some cationic complexes were able to cross membrane of live cells but they end up in lysosomes or stick to the mitochondrial membrane,[20,25] a common pitfall for the positively charged luminescent probes for live cell imaging. Indeed, targeting other organelles and the cytosol is challenging.[28] To our knowledge, controlled delivery of lanthanide complexes to the cytosol of live cells or to organelles other than lysosomes or mitochondria has rarely been achieved.[29–37] Most of these examples relies on the conjugation of the Ln^{3+} complex to a cell penetrating peptide (CPP).[31–33,35–37]

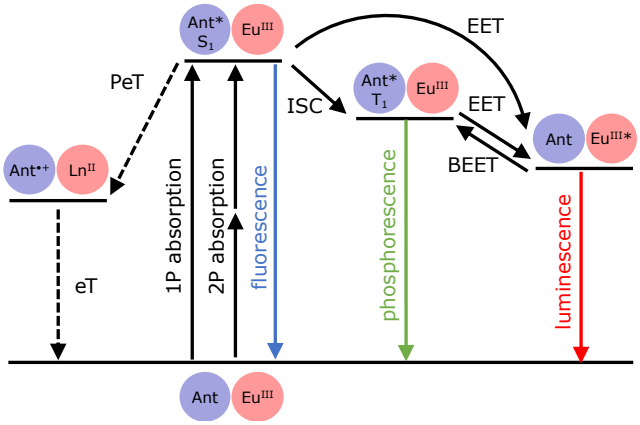

Figure 1. Jablonski-Perrin diagram of Eu^{3+} complexes with sensitizing antenna (Ant), showing pertinent photophysical processes (ISC = intersystem crossing, EET = electronic energy transfer, BEET = back electronic energy transfer, PeT = photoinduced electron transfer, eT = electron transfer).

We have recently used this strategy to design several Ln^{3+}-based probes for 2PM that are delivered to the cytosol of live cells. The first one was **ZF5.3[Tb(L1)]**,[36] a conjugate between a Tb^{3+} complex and ZF5.3, a CPP that is efficient at delivering various cargoes, including small molecules, peptides or proteins, to the cytosol of live cells.[38,39] As a Tb^{3+} chelator, we chose a DO3Apic derivative, comprising a cyclen macrocycle with three acetate and one picolinate coordinating arms. DOA3pic forms a stable complex with Ln^{3+} and presents interesting luminescent properties.[40,41] The picolinate was equipped with an extended π-system that forms an alkoxy-aryl-picolinate push-pull antenna for 2P absorption. 2PM imaging of life cells after incubation with **ZF5.3[Tb(L1)]** showed unambiguous internalization and cytosol delivery of the conjugate, with characteristic diffuse Tb^{3+} emission in the entire cell, including the nucleus. We have also described a family of 2PM probes, named **dTAT[Ln·L]** and inspired by dfTAT, a dimer of the TAT (transactivator of transcription of human immunodeficiency virus) CPP with appended (tetramethyl)rhodamine dyes. dfTAT enters into live cells by endocytosis and escapes the endosomes to reach the cytosol.[37] **dTAT[Ln·L]** probes rely on the same TAT dimer as dfTAT but the rhodamine dyes are replaced by Ln(DO3Apic) complexes with π-extended picolinate antennae for 2P absorption. These probes are efficiently delivered to the cytosol of live cells allowing 2PM with either Tb^{3+} or Eu^{3+} as a Ln^{3+}.[37]

Most antenna used in this work were based on amido/alkoxy-phenyl-picolinate. They display an absorption charge transfer (CT) band with a maximum at 310-320 nm that extends hardly above 360 nm. Therefore, 2P excitation at 720 nm with a Ti:sapphire laser corresponded to the red-tail of the absorption band and was of very low efficiency. Our efforts to red-shift the excitation with an alkoxy-aryl-alkynyl-picolinate antennae (λ_{max} = 335 nm, $\lambda_{cut\text{-}off}$ = 380 nm)[20] were in vain because the alkyne function undergoes a side reaction during the probe synthesis (hydration or thiol-yne reaction). These modifications of the alkyne group kill the sensitization process.[36]

In 2020, de Bettencourt-Dias described two luminescent Ln^{3+} complexes based on a dipicolinate or a pyridine moiety substituted by a (*N*-carbazolyl)-aryl-alkynyl group to form push-pull antennae.[42] These two antennae displayed high 2P absorption cross-section (*ca*. 250 GM per antenna) and were able to sensitize Eu^{3+} and Yb^{3+} emission in DMSO or water/DMSO mixtures. Their CT band has a maximum around 350 nm and extend up to *ca*. 400 nm. In order to evaluate the potential of such an antenna in the context of 2PM imaging of live cells, we prepared conjugates comprising (i) a cell penetrating peptide and (ii) a Eu^{3+} complex that features a carbazole-based push-pull antenna, and characterized their photophysical properties. Taking into account the above-mentioned reactivity issues with alkyne groups, we decided to use both an antenna with the alkyne group and another one lacking this function. For this purpose, both *N*-carbazolyl-phenyl-alkynyl-picolinate and *N*-carbazolyl-phenyl-picolinate pendants were grafted onto a DO3A macrocycle in order to act as a long-wavelength absorbing antenna for Eu^{3+} (Figure 2). In this article, we describe the luminescence, non-linear optical properties and 2PM imaging properties of three conjugates comprising the carbazole-based Eu^{3+} complex and a CPP. Three different CPP were used: (i) TAT, a well-known CPP derived from HIV,[43] (ii) its dimeric derivative dTAT[44] and (iii) ZF5.3. We show that the complex with the antenna lacking the alkyne group has better luminescence properties in purely aqueous buffers. Interestingly, we also highlight that the peptide scaffold has a strong impact on the luminescence properties of the probe, its cytotoxicity and its intracellular localization.

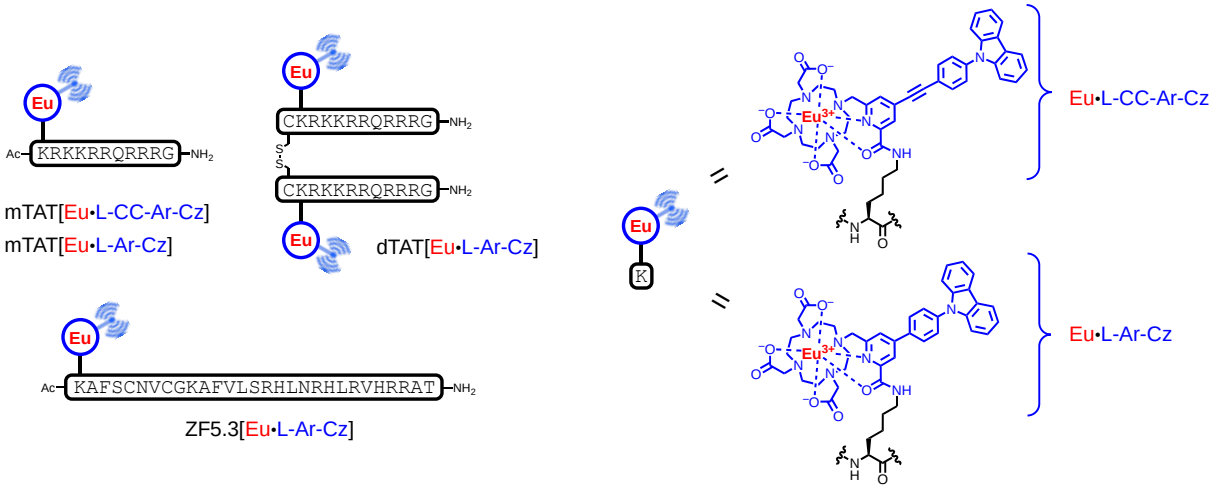

Figure 2. Chemical structure of the CPP/Ln complex conjugates used in this study. The Eu^{3+} ion is shown in red. L denotes the DO3A(picolinamide) moiety, CC-Ar-Cz and Ar-Cz denote the *N*-carbazolyl-phenyl-alkynyl and *N*-carbazolyl-phenyl substituents. The entire ligand is shown in blue, the CPP is represented as the black box, with its sequence inside.

Results and discussion

Design and synthesis of the luminescent probes: We have recently described several probes comprising a Ln(DO3Apic) complex conjugated to a peptide.[37] Conjugation can be performed using a carboxylate function introduced into the electron-donating group of the antenna[36] or using the carboxylate of the picolinate moiety,[37] which is transformed into a picolinamide after coupling to a lysine side chain. For carbazole-based systems, the picolinate moiety was chosen as the peptide conjugation site (Figure 2). The syntheses of pro-ligands **L-CC-Ar-Cz(tBu)$_3$** and **L-Ar-Cz(tBu)$_3$** (Figure 3) were performed starting from compound **1**,[37] a cyclen derivative with picolinate and acetate arms protected as methyl and *t*-butyl esters, respectively. The *t*Bu-protected pro-ligand **L-CC-Ar-Cz(*t*Bu)$_3$** was obtained in 57% yield by a Sonogashira coupling with compound **2** (obtained from commercially available 9-(4-bromophenyl)-9H-carbazole) followed by hydrolysis of the picolinate methyl ester and HPLC purification. The Sonogashira coupling was performed under modified conditions *i.e.*, in the absence of Cu(I) to avoid formation of macrocycle–copper complex that cannot be separated from the target compound and in the presence of tetrabutylammonium fluoride (TBAF) for *in situ* deprotection of the alkyne group. The pro-ligand **L-Ar-Cz(*t*Bu)$_3$** was obtained in 55 % yield by Suzuki-Miyaura coupling between compounds **1** and **3** using polymer-bound $Pd(PPh_3)_4$ as a catalyst and subsequent hydrolysis of the methyl ester and HPLC purification. At this stage, we tried to prepare the Eu^{3+} complexes of **L-Ar-Cz** and **L-CC-Ar-Cz** but they were insoluble in most tested solvents including water, precluding photophysical characterization. For this reason, the complexes were conjugated to charged peptides in order to study their properties in purely aqueous buffer, which was our purpose.

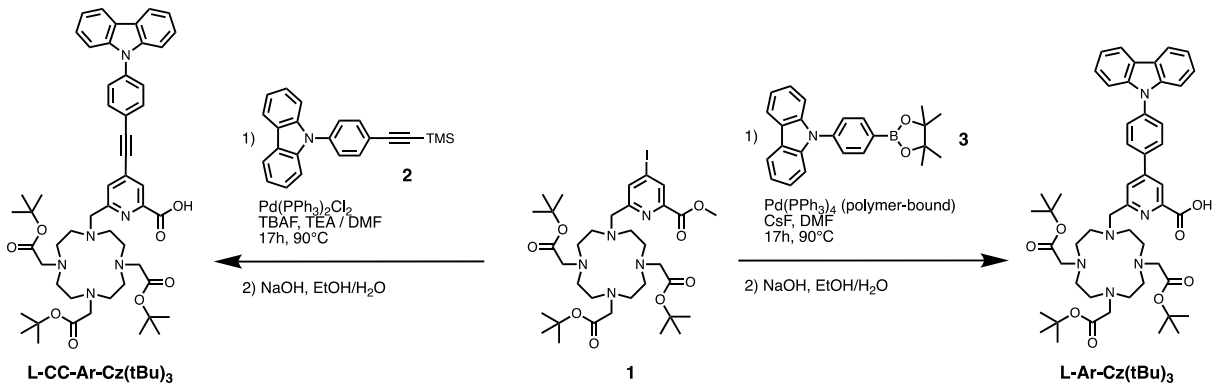

Figure 3. Synthesis of pro-ligands L-CC-Ar-Cz(tBu)$_3$ and L-Ar-Cz(tBu)$_3$.

The synthesis of the Ln^{3+} complex-CPP conjugates in shown in Figure 4. The three peptides were elongated on Rink Amide resin using standard protocols for solid phase peptide synthesis (SPPS) with the Fmoc/tBu strategy. A lysine with its side chain protected with an alloc group was introduced in the sequence where the Ln^{3+} complex will be grafted. The alloc protecting group is orthogonal to the other standard amino acid protecting groups. It was selectively removed on resin using Pd^0. Then, **L-Ar-Cz(*t*Bu)$_3$** was coupled through the picolinic acid to the unprotected lysine using PyBOP/DIEA activation, leading to a picolinamide. After acidic cleavage from the resin and removal of side chain protecting groups in a mixture of TFA and scavengers (water, triisopropylsilane and thioanisole), the peptide with the appended ligand was purified by HPLC. Note that extensive TFA/scavenger treatment (at least 4-5 h) was required for complete acidolysis of the *t*Bu esters of the macrocyclic ligand. Metalation with Eu^{3+} was performed using excess $EuCl_3$ in aerated water at pH 8.5 during 15 h for **mTAT[Eu·L-Ar-Cz]** and **ZF5.3[Eu·L-Ar-Cz]** but during two days for **dTAT[Eu·L-Ar-Cz]** to ensure the completeness of the concomitant formation of the disulfide bond (Figure 4). In the case of **ZF5.3[Eu·L-Ar-Cz]**, the disulfide that may have formed were reduced with TCEP prior to HPLC purification. In the case of the alkyne-containing antenna, only the conjugate **mTAT[Eu·L-CC-Ar-Cz]** was prepared (*vide infra*). The Ln^{3+} complex-CPP conjugates were obtained pure after HPLC purification and freeze drying and they were identified by ESI-MS analysis (Figure S1 of Supporting Information). All conjugates are soluble in water (at least below 250 µM) due to the highly charged peptide scaffold. Interestingly, we did not observe any addition of water or thioanisole (used as a scavenger in TFA treatment) on the alkyne group during the synthesis of **mTAT[Eu·L-CC-Ar-Cz]**. We have previously observed nucleophile addition on the alkyne group of related molecules with an alkoxy or dialkylamino *para* donor group but not in this case with the carbazole donor.[36] Indeed, the alkyne group might be activated in acidic conditions by protonation of both the picolinate moiety and the electron-donating group which is not possible with carbazole due to its low basicity.

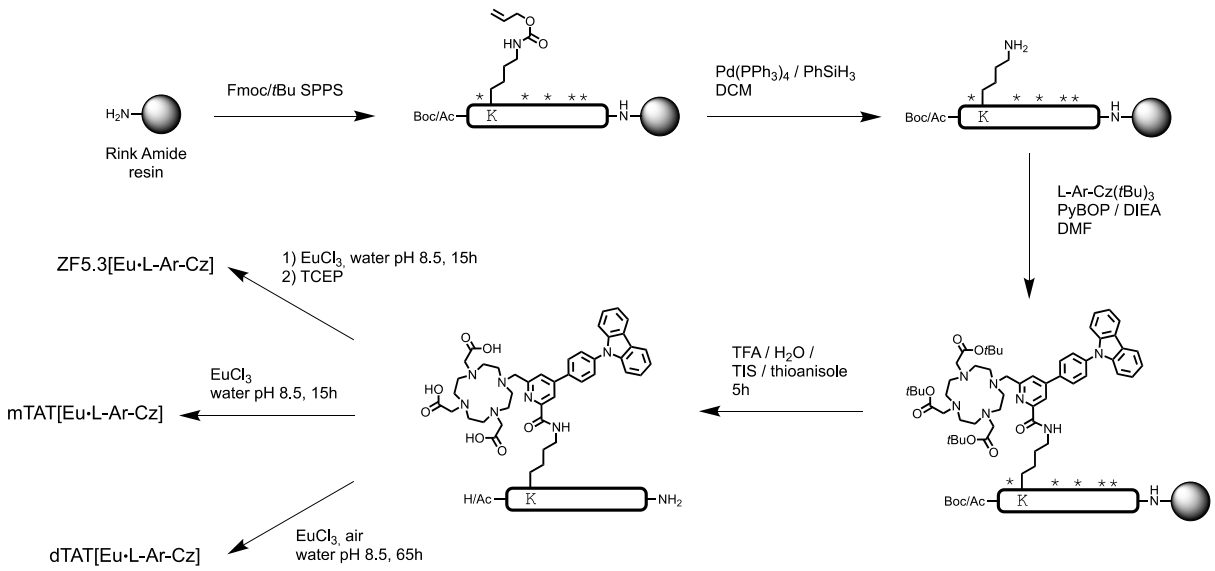

Figure 4. Synthetic pathway for **mTAT[Eu·L-Ar-Cz], dTAT[Eu·L-Ar-Cz] and ZF5.3[Eu·L-Ar-Cz]**. The CPP is shown as a black box and only the lysine serving as the grafting point is shown. * denotes standard protecting groups for Fmoc/*t*Bu SPPS.

Photophysical properties in PBS: The photophysical properties of **mTAT[Eu·L-CC-Ar-Cz]** and **mTAT[Eu·L-Ar-Cz]** were studied comparatively in a purely aqueous medium, *i.e.* phosphate buffer saline (PBS, pH 7.4). Their absorption, emission and excitation spectra are shown in Figure 5 and relevant spectroscopic data are summarized in Table 1. The absorption spectrum of **mTAT[Eu·L-CC-Ar-Cz]** shows several bands that can be attributed to the carbazole locally excited (LE) transitions (287, 320 and 340 nm; Figure S3) together with a broad absorption band with a maximum at 362 nm that is attributed to a CT transition in the *N*-carbazolyl-phenyl-alkynyl-picolinate antenna. This low-energy band extends up to 433 nm ($\lambda_{cut\text{-}off}$). Upon excitation in the CT band at 362 nm, the characteristic Eu^{3+} emission is observed with $^5D_0 \rightarrow {}^7F_J$ (J = 0, 1, 2, 3, 4) transitions at 580, 590, 615, 650, and 700 nm, together with a weaker but broad residual fluorescence emission from the antenna (λ_{max} = 455 nm, $\Phi_L = 2\times10^{-4}$). The Eu^{3+} excitation spectrum matches well the absorption spectrum indicating that both the antenna LE and CT transitions of the antenna sensitize Eu^{3+} emission. The quantum yield of the Eu^{3+} emission is very weak (Φ_{Eu} = 0.0013). The absorption spectrum of the other carbazole-based conjugate, **mTAT[Eu·L-Ar-Cz]**, resembles that of **mTAT[Eu·L-CC-Ar-Cz]** with both LE (carbazole-based) and CT contributions but the CT band is blue-shifted by *ca.* 15 nm and extend up to 420 nm. Excitation in the CT band at 350 nm yields the classical Eu^{3+} emission, whose spectrum is identical to that of **mTAT[Eu·L-CC-Ar-Cz]** due to the same chelator, *i.e.* same symmetry around Eu^{3+}. The residual antenna fluorescence emission is weak. The Eu^{3+} excitation spectrum is in good agreement with the absorption spectrum confirming Eu^{3+} sensitization through the *N*-carbazolyl-phenyl-picolinamide antenna. The quantum yield of Eu^{3+} emission, Φ_{Eu}, is weak, 0.0017, and slightly higher than the alkyne-containing analogue. In addition, the Eu^{3+} luminescence lifetime of **mTAT[Eu·L-Ar-Cz]** is slightly longer (Table 1 and Figure S5). However, related [Eu·DO3Apic] complexes (conjugated to peptide or not) having antennas with higher energy absorption show much higher Eu^{3+} emission quantum yields (Φ_{Eu} ~ 0.15) and luminescence lifetimes (τ_{Eu} ~ 1.1 ms) in PBS.[36,37,40,41]

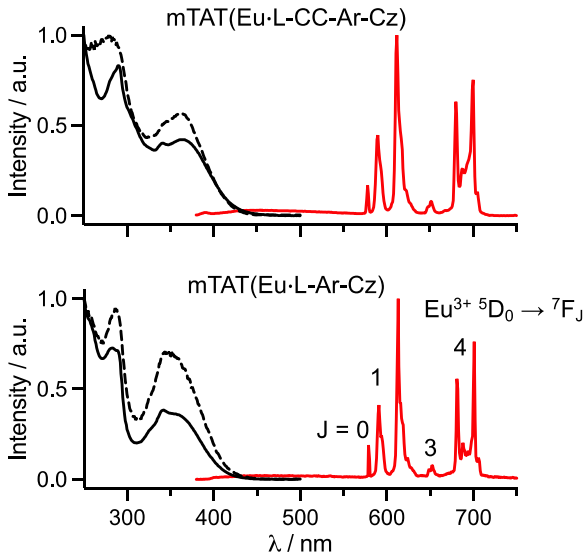

Figure 5. Normalized absorption (black solid line), emission (λ_{ex} = 350 nm; red solid line), Eu^{3+} excitation (λ_{em} = 615 nm; black dashed line) excitation spectra of **mTAT[Eu·L-CC-Ar-Cz]** and **mTAT[Eu·L-Ar-Cz]** dissolved in PBS.

Table 1. Spectroscopic characterizations of **mTAT[Eu·L]**, **mTAT[Eu·L]** and **ZF5.3[Eu·L]** conjugates in PBS (aerated solutions otherwise noted).[a]

Compound	λ_{max}; $\lambda_{cut\text{-}off}$ / nm	$E(S_1)$ $E(T_1)$[b] / cm^{-1}	ε at λ_{max} / $M^{-1}\,cm^{-1}$	Φ_L $\times10^2$	Φ_{Eu} $\times10^2$	τ_{Eu} (H_2O, aerated); τ_{Eu} (H_2O, de-oxygenated); τ_{Eu} (D_2O, aerated) / ms	q
mTAT[Eu·L-CC-Ar-Cz]	362; 433	S_1: 23100 T_1: 20400	37000	0.02	0.13	0.37 (59%), 0.87 (41%); 0.38 (63%), 0.89 (37%); 0.45 (70%),1.20 (30%)	0.0 / 0.2[b]
mTAT[Eu·L-Ar-Cz]	345; 420	S_1: 23800 T_1: 21400	15000	0.01	0.17	0.80; 0.82; 1.12	0.0
dTAT[Eu·L-Ar-Cz]	360; 424	S_1: 23600	–	0.01	0.20	0.40 (46%), 0.87 (54%); –; –	–
ZF5.3[Eu·L-Ar-Cz]	345; 423	S_1: 23400	–	0.1	1.4	1.01; –; –	–
ZF5.3[Eu·L-Ar-Cz]+Zn	345; 422	S_1: 23700	–	0.1	1.8	1.08 –; –	–

[a] Error is estimated ± 5% on ε values and ± 10% on Φ_{Ln}. Error on τ_{Ln} is estimated ± 0.03 ms. Error on *q* is estimated ± 0.2. Energy of the excited triplet state is estimated from the wavelength at half-maximum on the onset of the time-gated phosphorescence spectrum of the Gd^{3+} analogue in PBS/glycerol 9:1 v/v recorded at 77 K. ε values were determined from titrations of the free ligand with a Ln^{3+} salt (details in the Supporting Information). [b] *q* values were determined using Parker's equations[45] $q^{Eu} = 1.2\times(1/\tau_{Eu}(H_2O) - 1/\tau_{Eu}(D_2O) - 0.325))$ with τ in ms. The first value is determined with the shorter lifetime, the second one with the longer lifetime.

In order to get more insight into the weak Eu^{3+} emission quantum yields in PBS of these two conjugates, the photophysical properties were investigated further. Ln^{3+} excited states are quenched by overtones of O-H vibrations and the number of water molecules coordinated to the Ln^{3+} ion is a critical parameter for the emission efficiency. The DO3Apic chelator offers a 9-atom coordination set that is expected to saturate the Eu^{3+} coordination sphere. The number of coordinated water molecules, *q*, was determined to be 0 for both conjugates

from measurement of the Eu^{3+} emission decay lifetimes in PBS solution in H_2O and D_2O.[45] This indicates that water coordination is not responsible for the low Φ_{Eu} value. In aerated solution, thermally activated back energy transfer from the Ln^{3+} excited state to the antenna T_1 state may also quench Ln^{3+} emission. The energy values of the antenna T_1 state were measured with the Gd^{3+} analogues **mTAT[Gd·L-CC-Ar-Cz]** and **mTAT[Gd·L-Ar-Cz]** (Figure S6) and were found at 20400 and 21400 cm^{-1}, respectively. This is more than 3000 and 4000 cm^{-1} above the Eu^{3+} $^5D_0$ emissive excited state, respectively, precluding significant thermally activated back energy transfer. This is confirmed by very similar Eu^{3+} emission lifetimes in aerated and de-oxygenated solutions (Table 1) for each conjugate.

Solvent dependance of the emission: Both conjugates are very weakly emissive ($\Phi_{Eu} < 0.002$) in a purely aqueous solution, in contrast with the quantum yields reported by De Bettencourt-Dias for related Eu^{3+} complexes with a carbazole antenna in pure DMSO ($\Phi_{Eu} \approx 0.3$) or a DMSO/water mixture ($\Phi_{Eu} \approx 0.03$). Thus, they were further characterized in an organic solvent, DMF, which readily dissolves peptides (Table 2). Their absorption spectra (Figure S7) are similar to those in PBS, with both LE and CT bands but the CT band in blue-shifted in DMF as compared to PBS, in agreement with the lower polarity of DMF. Under 350 nm excitation, characteristic Eu^{3+} emission is observed together with a broad and intense fluorescence band with maximum at 500 and 470 nm for **mTAT[Eu·L-CC-Ar-Cz]** and **mTAT[Eu·L-Ar-Cz]**, respectively (Figure S7). For the former conjugate, the antenna fluorescence emission dominates the emission spectrum ($\Phi_L = 0.21$ and $\Phi_{Eu} = 0.074$) while for the latter, Eu^{3+} emission dominates ($\Phi_L = 0.047$ and $\Phi_{Eu} = 0.13$). Therefore, in DMF, the Eu^{3+} emission is more intense than in PBS but so is the antenna fluorescence. For both conjugates, the Eu^{3+} excitation spectrum (recorded with detection at 615 nm) corresponds well with the absorption, with the LE and CT component sensitizing Eu^{3+}. From these characterizations in PBS and DMF, it appears that **mTAT[Eu·L-Ar-Cz]** has superior Eu^{3+} emission properties and it might be more interesting for imaging studies.

Table 2. Spectroscopic characterizations of mTAT[Eu·L] conjugates in DMF.

Compound	λ_{max} ; $\lambda_{cut\text{-}off}$ / nm	$E(S_1)$ / cm^{-1}	Φ_L	Φ_{Eu}	τ_{Eu} / ms
mTAT[Eu·L-CC-Ar-Cz]	342; 420	S_1: 23800	0.21	0.074	1.16
mTAT[Eu·L-Ar-Cz]	342; 413	S_1: 24200	0.047	0.13	1.25

Carbazoles are known to be good electron donors that are widely used in optoelectronic devices for instance.[46] It has been proposed that photoinduced electron transfer (PeT) from the excited antenna to Eu^{3+} can be a competitive pathway to the electronic energy transfer that sensitize Eu^{3+} emission (Figure 1).[47,48] PeT efficiency is expected to depend on solvent polarity, which could account for the difference observed between PBS and water. De Bettencourt-Dias et al. have reported that the Eu^{3+} emission of their carbazole-based complexes depends on the solvent viscosity.[42] In order to gain a deeper insight into the low Eu^{3+} emission in PBS, **mTAT[Eu·L-Ar-Cz]** was studied in solvent mixtures with various polarity and viscosity, i.e. dioxane/water and acetonitrile/water mixtures. Quantum yields of the Eu^{3+} emission in these solvents were measured. Figure 6 shows the plots of $\log(\Phi_{Eu})$ against viscosity, in (A), or against $E_T(30)$, Reichardt's solvent polarity parameter,[49] in (B). Clearly no correlation is observed between viscosity and Eu^{3+} emission quantum yield while Φ_{Eu} decreases exponentially with polarity. This could be explained by a competitive PeT quenching process. In order to evaluate this, the Gibbs energy of this PeT was evaluated using Equation (1).[50–53]

$$\Delta G_{eT}{}^0 = (E^0{}_D - E^0{}_A) - E(S_1) - e^2/\varepsilon \quad (1)$$

where $E^0{}_D$ is the oxidation potential of the electron donor (carbazole), $E^0{}_A$ is the reduction potential of the acceptor (Eu^{3+}), $E(S_1)$ is the excited state energy of the antenna. The last term accounts for coulombic

interactions within the donor/acceptor pair after electron transfer, which can be estimated *ca.* 0.15 eV.[51–53] E^0_D and E^0_A were determined from model compounds (Supporting Information). The oxidation potential of the carbazole group in DMF is +1.5 V / NHE, in agreement with the literature.[46] Electrochemical measurements show that the reduction potential of the picolinate moiety and Eu^{3+} are very similar, at *ca.* –1.2 V / NHE (Supporting Information), in agreement with literature.[48,52,52,54] From the S_1 energy value in Table 1, a value of *ca.* –0.4 eV is calculated $\Delta G_{eT}{}^0$ from carbazole to Eu^{3+}. This indicates that the PeT process is thermodynamically favored and can potentially compete with the energy transfer pathway, thereby accounting for the low Φ_{Eu} measured in PBS.

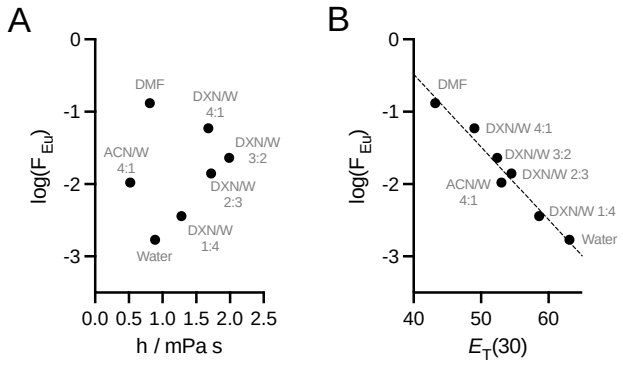

Figure 6. Dependence of Eu^{3+} emission quantum yield on (A) viscosity and (B) $E_T(30)$ solvent polarity parameter. ACN = acetonitrile; DXN = dioxane; W = water. Details are given in the Supporting Information.

Two-photon absorption properties: De Bettencourt-Dias have reported 2P absorption cross values, σ_{2P}, of about 250 GM per antenna at 750 nm in the case of Eu^{3+} complexes with dipicolinate or a pyridine substituted by a (*N*-carbazolyl)-aryl-alkynyl as antennas. A similar value is thus expected for **mTAT[Eu·L-CC-Ar-Cz]** with the mono-picolinate antenna. The impact of removing the alkynyl group was evaluated by determining the 2P absorption cross-section of **mTAT[Eu·L-Ar-Cz]**. As the Eu^{3+} emission quantum yield is low in PBS, two-photon excited fluorescence measurements were performed in MeCN/water 4:1 (v/v), following a procedure described before (Φ_{Eu} = 0.011 in MeCN/water 4:1 (v/v)).[37] Upon excitation at 730 nm, with a Ti:sapphire laser, classical Eu^{3+} emission is detected and a quadratic dependance of the emission intensity on the laser power confirmed the biphotonic excitation (Figure 7A). The 2P absorption spectrum is shown in Figure 7B. The low-energy end of the spectrum, above 760 nm, matches well the CT band of the wavelength-doubled 1P absorption spectrum but, the agreement is poorer below 760 nm. This indicates that the CT transition that sensitize Eu^{3+} luminescence is 2P allowed but 2P excitation and sensitization through the LE state is less efficient. At 750 nm, the 2P cross section value is 100 GM, *ca.* 2.5 times lower than the value determined for the antenna with the alkynyl group. Nevertheless, the *N*-carbazolyl-phenyl-picolinate antenna of **mTAT[Eu·L-Ar-Cz]** outperforms similar antennas with methoxy or acetamido donors instead of the carbazole one that we have described recently.[37] For comparison, these antenna have σ_{2P} values in the range 4-12 GM at 700 nm and a cut-off value for 2P absorption at *ca.* 730 nm. In 2PM experiments, the 2P absorption properties of the carbazole-based system might compensate for the lower quantum yield. Additionally, the long-wavelength 2P absorption that extends up to 850 nm may be advantageous for 2P microscopy. The main contributors to 2P-excited cell autofluorescence are NAD(P)H and FAD, with 2P absorption λ_{max} of 720 and 750 nm respectively, and 2P $\lambda_{cut\text{-}off}$ of *ca.* 800 and 850 nm, respectively.[55,56] As compared to previously reported **dTAT[Eu·L]** probes with methoxy/acetamido-aryl-picolinate antennas, which are excitable only below 730 nm, the carbazole-based antenna allows 2P

excitation at 800 nm or above, which is an advantage to reduce cell autofluorescence arising from NAD(P)H and FAD.

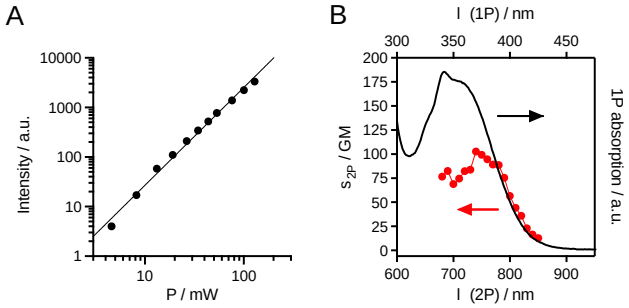

Figure 7. (A) Quadratic power dependance of the Eu^{3+} emission (λ_{ex} = 730 nm) for **mTAT[Eu·L-Ar-Cz]** in MeCN/water 4:1 (v/v). Data were fitted using $I = A \times P^n$ yielding n = 1.97. (B) Superimposition of the 2P absorption spectrum (lower abscissa for wavelength, red dots) and 1P absorption spectrum (upper abscissa, black solid line) for **mTAT[Eu·L-Ar-Cz]** in MeCN/water 4:1 (v/v).

Influence of the peptide scaffold on the luminescence properties: The luminescence properties of conjugates **dTAT[Eu·L-Ar-Cz]** and **ZF5.3[Eu·L-Ar-Cz]** were determined and compared to those of **mTAT[Eu·L-Ar-Cz]**. The former shows absorption, excitation and emission spectra that are very similar but the CT band is slightly more intense and red-shifted as compared to the LE bands (Figure S8 and Table 1). A bi-exponential Eu^{3+} decay is observed with lifetimes values of 0.40 and 0.87 ms (Table 1). The Eu^{3+} emission quantum yield remains very low (Φ_{Eu} = 0.0019). Therefore, dimerization of the TAT conjugate has only little influence on the Eu^{3+} emission properties. ZF5.3 is a classical ββα zinc finger peptide that binds one Zn^{2+} ion.[38,39] Such zinc finger peptides are random coils with no defined conformation in the Zn^{2+}-free form, but they adopt a ββα fold in their Zn^{2+}-bound form, with a short β-hairpin and a α-helix.[57,58] Hence, **ZF5.3[Eu·L-Ar-Cz]** was characterized in its Zn^{2+}-free and Zn^{2+}-bound forms (Table 1). Subtle changes in the absorption spectrum are observed upon Zn^{2+} binding, with a slight blue-shift of the CT band but the Eu^{3+} emission spectrum remains unchanged (Figure S9). These spectra are similar to those of the mTAT and dTAT analogues. However, the quantum yield of Eu^{3+} emission is 0.014 and 0.018 for the Zn^{2+}-free and Zn^{2+}-loaded forms, respectively, values that are *ca.* 10 times higher than for the mTAT and dTAT analogues. In agreement with the higher quantum yield, the lifetime of Eu^{3+} emission is higher (1.01 and 1.08 ms for the Zn^{2+}-free and Zn^{2+}-loaded forms, respectively). Since the Eu^{3+} emission quantum yield of the carbazole-based complex depends on polarity, these changes may be attributed to variation in the environment of the carbazole antenna within the various conjugates. Indeed, contrary to the TAT peptide, ZF5.3 has several hydrophobic amino acids that may interact with the antenna, both in the unstructured Zn^{2+}-free and folded Zn^{2+}-bound forms of ZF5.3. In the Zn-bound form, these amino acids are packed on one side of the peptide, exposed to solvent and close to the N-terminus where the Eu^{3+} complex is grafted (Figure S11). Therefore, the hydrophobic antenna may interact with these hydrophobic amino acids, leading to a more emissive complex in the case of ZF53.

Two-photon microscopy: Before carrying out microscopy, MTT proliferation assay was used to assess the cytotoxicity of **mTAT[Eu·L-Ar-Cz], dTAT[Eu·L-Ar-Cz]** and **ZF5.3[Eu·L-Ar-Cz]** (Zn^{2+}-bound and free) after 1 h incubation in RPMI culture medium (without serum) and 24 h proliferation in RPMI with serum, following a previously reported procedure.[37] Among the three conjugates, **dTAT[Eu·L-Ar-Cz]** is the most toxic, with an IC50 value of 2.3 µM, which is significantly lower than other TAT dimers with appended Ln complexes with methoxy/acetamido-aryl-picolinate antennas that we have described recently (IC50 ≈ 10-20

µM).[37] This suggests that the carbazole donor group adds some toxicity to the system, possibly due to its high lipophilicity (*vide infra*). **mTAT[Eu·L-Ar-Cz]** is less toxic (IC50 = 8 µM). Zn-bound **ZF5.3[Eu·L-Ar-Cz]** is the least toxic of the series with an IC50 value above 25 µM but, interestingly, in its Zn-free form, it is much more toxic (5.5 µM). Cell staining properties of these conjugates were studied by two-photon microscopy with HeLa cells.

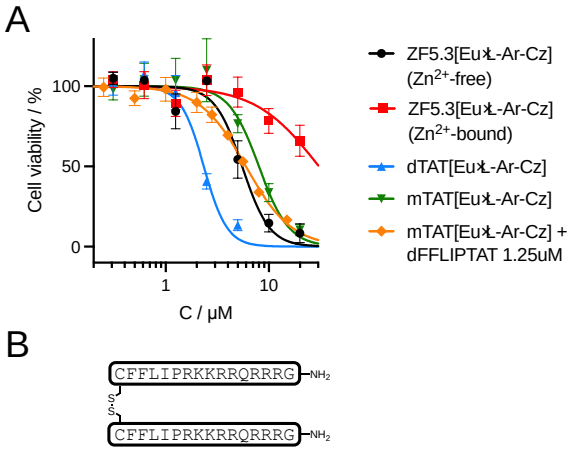

Figure 8. (A) MTT proliferation assay with HeLa cells (1 h incubation in RPMI without serum and 24 h proliferation in RPMI with 10 % fetal calf serum). Symbols correspond to experimental data and solid lines to the fit that yielded IC50 values given in Table 3. Error bars correspond to the SEM. (B) Chemical structure of dFFLIPTAT.

Table 3. Half maximal inhibitory concentration, IC50, determined from MTT proliferation assays.

Compound	IC50 / µM
mTAT[Eu·L-Ar-Cz]	8 ± 2
dTAT[Eu·L-Ar-Cz]	2.3 ± 0.3
ZF5.3[Eu·L-Ar-Cz], Zn^{2+}-bound	> 25
ZF5.3[Eu·L-Ar-Cz], Zn^{2+}-free	5.5 ± 0.9
mTAT[Eu·L-Ar-Cz] + dFFLIPTAT 1.25 µM	6.0 ± 0.6

For 2PM, cells were incubated 1 h in RPMI medium with each conjugate at a concentration that shows ≥ 90% cell viability, according to MTT proliferation assay, washed and analyzed. Biphotonic excitation was performed at 800 nm, in order to reduce autofluorescence arising from NADH and FAD. With **dTAT[Eu·L-Ar-Cz]** (1 µM), a punctate Eu^{3+} emission is detected in almost all cells, as attested by spectral detection (Figure 9). This suggests endosomal entrapment of the Eu^{3+} probe at this concentration. Indeed, endosomal entrapment has been reported by Pellois et al. for dfTAT at low concentration (< 5 µM)[44] and by us for related **dTAT[Ln·L]** probes when incubated below 5 µM also.[37] In addition to the Eu^{3+} puncta, larger clumps with Eu^{3+} emission are also observed, which may correspond to probe aggregates on the cell surface. Eu^{3+} emission is also detected in the in areas where there are no cells, possibly due to the dissolution of aggregates after washing or to the probe adsorbed on the glass surface. Eu^{3+} emission arising from the nucleus is very low, well below the level of extracellular emission. The strong toxicity of **dTAT[Eu·L-Ar-Cz]** precluded the use of a higher incubation concentration for live cell imaging, that would allow cytosolic delivery as observed with the previously reported **dTAT[Ln·L]** probes with methoxy-aryl or acetamido-aryl substituents on the picolinate.[37] Nevertheless, incubation was attempted at 5 µM, despite obvious toxicity. The 2PM images are shown in Figure S12 of the

Supporting Information. The DIC image shows rounded and swelled HeLa cells with turbid nuclei, often indicative of dying cells. Diffuse Eu^{3+} emission is observed in the cytoplasm and in the nucleoli but not in the nucleoplasm. Interestingly, the Eu^{3+} emission is also detected at the cell membrane, and it is stronger than in the cytoplasm. As the Eu^{3+} emission of the probe is polarity-dependent, this suggests that the carbazole moiety is inserted into the lipid layer of the membrane and probably destabilize it, causing cell death.

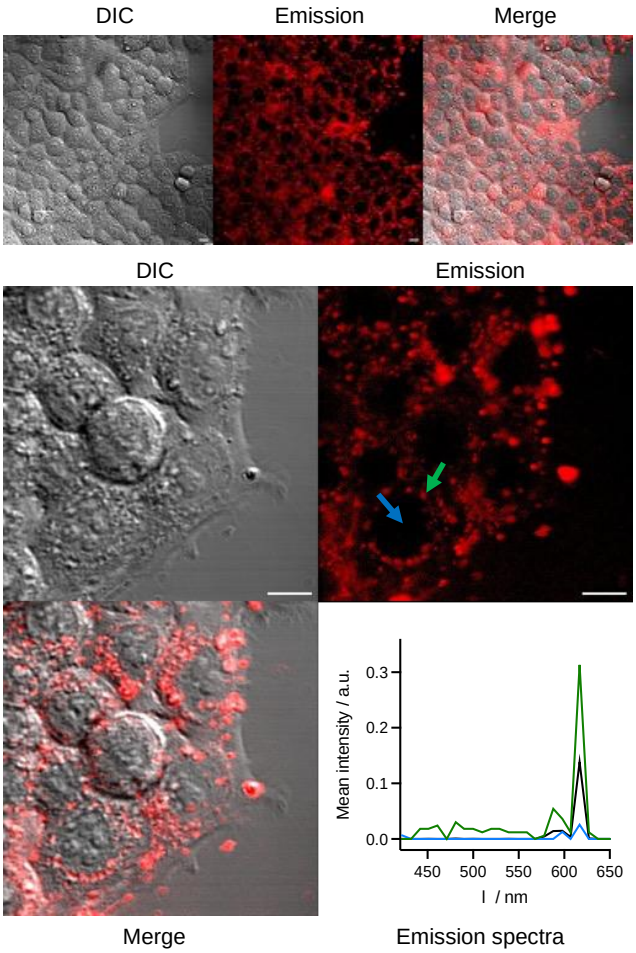

Figure 9. 2PM imaging (λ_{ex} = 800 nm) of living HeLa cells incubated 1 h with **dTAT[Eu·L-Ar-Cz]** (1 µM) in RPMI medium. (Top) Wide field images; *Left panel:* differential interference contrast (DIC); *Middle panel*: luminescence recorded using a 420-690nm bp filter and APD detection; *Right panel:* merge. (Bottom) zoom images (DIC, emission and merge) and mean 2P-excited emission spectra (detected with a PMT array) of perinuclear puncta (green), nucleus (blue) and extracellular area (black). Scale bars correspond to 10 µm.

For Zn-bound **ZF5.3[Eu·L-Ar-Cz]**, the incubation was performed using a non-toxic concentration of 5 µM. Under 800 nm excitation, the Eu^{3+} emission is detected within all cells (Figure 10). Probe aggregates, which were not removed by washing, are also observed in the extracellular medium. The Eu^{3+} emission in cells seems to arise from large vesicles around the nucleus as shown by overlay of DIC and Eu^{3+} emission images. No Eu^{3+} emission is observed in the nucleus.

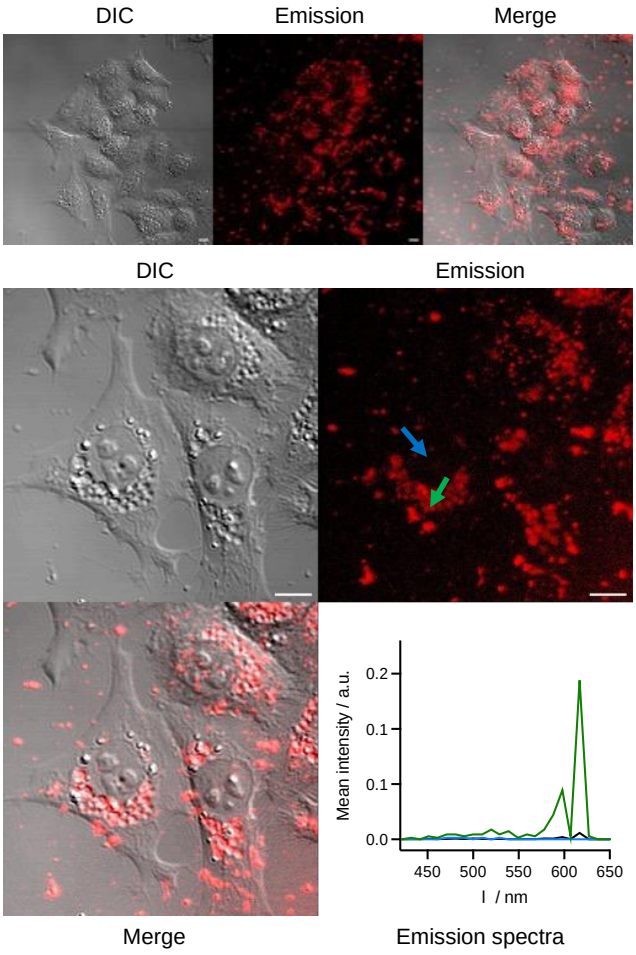

Figure 10. 2PM imaging (λ_{ex} = 800 nm) of living HeLa cells incubated 1 h with Zn-bound **ZF5.3[Eu·L-Ar-Cz]** (5 µM) in RPMI medium. (Top) Wide field images; *Left panel:* differential interference contrast (DIC); *Middle panel*: luminescence recorded using a 420-690nm bp filter and APD detection; *Right panel:* merge. (Bottom) zoom images (DIC, emission and merge) and mean 2P-excited emission spectra (detected with a PMT array) of perinuclear puncta (green), nucleus (blue) and extracellular aera (black). Scale bars correspond to 10 µm.

In the case of **mTAT[Eu·L-Ar-Cz]**, the incubation concentration was set at 2.5 µM. Only a few cells (*ca.* 5-10%) were stained with the Eu^{3+} probe (Figure 11A). In order to improve probe internalization, we opted for a co-incubation strategy described by Pellois et al. using a non-fluorescent dimeric TAT derivative, dFFLIPTAT (Figure 8B). This peptide was described as an endosomolytic agent, as was dfTAT, and it is able to deliver co-incubated species into the cytosol of live cells.[59] It is highly effective above 1 µM (> 50% cell stained) and shows low toxicity to MDA-MD-231 and Neuro-2a cells at 1.5 µM. We first evaluated the toxicity of dFFLIPTAT to HeLa cells by the MTT proliferation assay and found no toxicity below 1.5 µM (Figure S13). Secondly, MTT proliferation assay was performed with a mixture of dFFLIPTAT and **mTAT[Eu·L-Ar-Cz]**. The concentration of the former was fixed at 1.25 µM and the concentration of the latter was varied (Figure 8). An IC50 of 6.0 µM was found in this case (Table 3) and no significant toxicity was observed for the 1.25 µM dFFLIPTAT / 1.0 µM **mTAT[Eu·L-Ar-Cz]** mixture. Therefore, HeLa cells were incubated 1 h with this mixture before washing and 2PM analysis. Contrary to incubation with **mTAT[Eu·L-Ar-Cz]** alone, *ca.* 50 % of the cells were stained despite the lower Eu^{3+} probe concentration (Figure 11B). Eu^{3+} emission was detected in the whole cell, both outside and inside the nucleus, indicating proper and efficient cytosolic delivery of the probe using dFFLIPTAT for co-incubation. The Eu^{3+} emission is more intense in the perinuclear area, which in part

corresponds to mitochondria as shown by co-staining with MitoView 405, a mitochondria-specific dye (Figure S14). However, it is difficult to determine if the probe is more accumulated in the mitochondria or if its luminescence is increased due to localization in the lipid layer of the mitochondria membrane. Note that the staining pattern observed in the case of the co-incubation of **mTAT[Eu·L-Ar-Cz]** with dFFLIPTAT is similar to the one observed with **mTAT[Eu·L-Ar-Cz]** alone (Figure S15) but much more cells have internalized the probe in the presence of dFFLIPTAT.

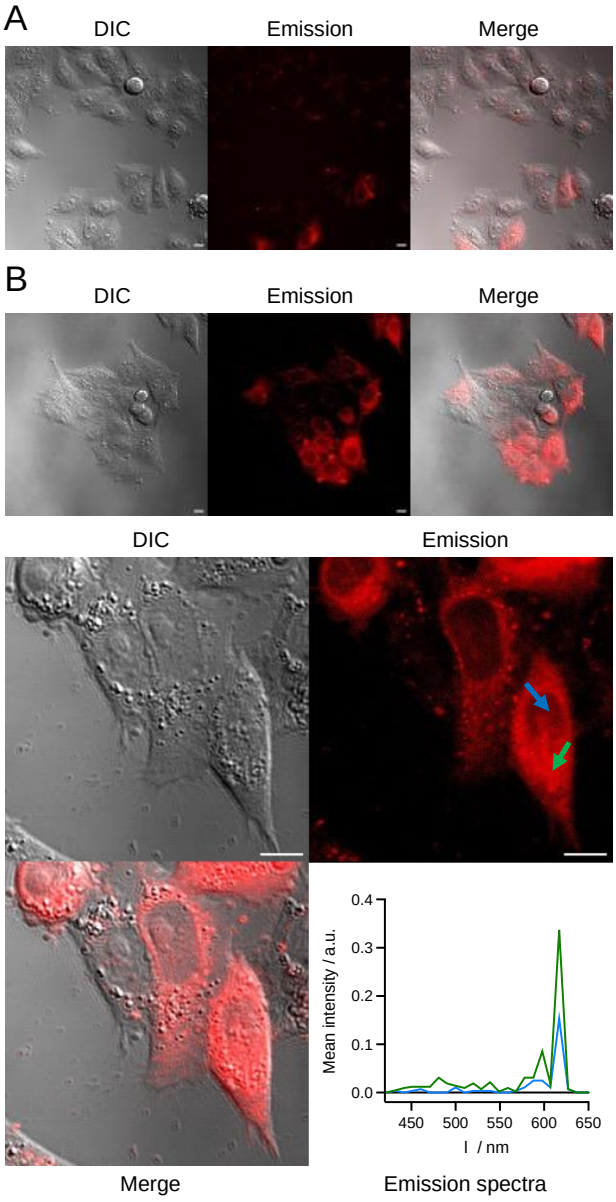

Figure 11. 2PM imaging (λ_{ex} = 800 nm) of living HeLa cells incubated 1 h with (A) **mTAT[Eu·L-Ar-Cz]** (2.5 µM) and (B) a mixture of **mTAT[Eu·L-Ar-Cz]** (1 µM) and dFFLIPTAT (1.25 µM) in RPMI medium. (A) Wide field images; *Left panel:* differential interference contrast (DIC); *Middle panel*: luminescence recorded using a 420-690nm bp filter and APD detection; *Right panel:* merge. (B) Wide field images; *Left panel:* DIC; *Middle panel*: emission; *Right panel:* merge. (Bottom) zoom images (DIC, emission and merge) and mean 2P-excited emission spectra (detected with a PMT array) in the perinuclear area (green), nucleus (blue) and extracellular area (black). Scale bars correspond to 10 µm.

Conclusion

The purpose of this article was to evaluate to potential of Eu^{3+} complexes containing carbazole-based antennas for 2PM imaging of live cells. We have studied two Eu^{3+} complexes based on a DO3Apic ligand with a π-extended picolinate antenna for 2P absorption. One of the complexes shows a *N*-carbazolyl-phenyl-alkynyl π-extension, first introduced by de Bettencourt-Dias et al. a few years ago,[42] and the other is a variant lacking the alkynyl group. These complexes were grafted onto a TAT cell penetrating peptide, which ensures solubility in water. Despite interesting absorption properties, with a CT band extending above 400 nm, both conjugates show poor emissive properties with quantum yields around 0.002 in PBS. In DMF, the Eu^{3+} emission quantum yields are much higher and the compound lacking the alkynyl group, **mTAT[Eu·L-Ar-Cz]**, shows the most interesting luminescence properties, especially a higher emission quantum yield. Indeed, a careful evaluation of its emission properties in various solvents revealed a clear dependence of the Eu^{3+} emission properties on solvent polarity. From our photophysical characterization, a likely mechanism to explain the low quantum yield in water is a PeT process from the excited antenna to the Eu^{3+} or the picolinamide moiety that can outcompete the sensitizing energy transfer in polar solvents. The Eu^{3+} complex that lacks the alkynyl group, **[Eu·L-Ar-Cz]**, shows less efficient 2P absorption properties than alkynyl-containing analogues with a carbazole donor. Nevertheless, it is interesting for 2PM compared to related complexes with methoxy or acetamido donating groups instead of carbazole: (i) the 2P absorption extends above 750 nm and up to 850 nm, which is interesting to minimize 2P autofluorescence and (ii) the 2P cross-section is rather high, with a value of 100 GM at 750 nm. For cellular studies, besides mTAT, two other CPP were equipped with **[Eu·L-Ar-Cz]**: dTAT, a dimer of TAT, and ZF5.3, a zinc finger peptide bearing the 5.3 penta-arginine motif. Interestingly, the latter which exposes a set of hydrophobic amino acids to interact with the carbazole antenna, offers a higher Eu^{3+} emission quantum yield, in agreement with the polarity-dependent emission. 2PM imaging of HeLa cells was performed at non-toxic concentrations, as determined by MTT proliferation assays, for all conjugates. Disappointingly, **dTAT[Eu·L-Ar-Cz]** and **ZF5.3[Eu·L-Ar-Cz]** showed only punctate/vesicular distribution around the nucleus, with no indication of proper cytosolic delivery. On the contrary, **mTAT[Eu·L-Ar-Cz]**, boosted by co-incubation with dFFLIPTAT, was delivered to the cytosol of live HeLa cells and Eu^{3+} could be detected within the whole cell, including nucleus. The most intense Eu^{3+} emission likely originates from mitochondria, possibly due to a higher quantum yield in the lipid membrane of the mitochondria, in agreement with the polarity-dependent emission properties of the **[Eu·L-Ar-Cz]** complex. At high and toxic concentration, cells incubated with **dTAT[Eu·L-Ar-Cz]** showed also intense Eu^{3+} emission at the extracellular membrane, revealing prolonged accumulation of the probe in the membrane, possibly destabilizing it. As a conclusion, despite its very low Eu^{3+} emission quantum yield in water, **[Eu·L-Ar-Cz]** with its carbazole-based push-pull antenna has interesting 2P absorption properties for 2PM imaging and can be delivered efficiently to the cytosol of live cells when conjugated to a TAT monomer, to give high-quality 2PM images.

Experimental section

Materials and methods. *N*-α-Fmoc-protected amino acids for peptide synthesis, HCTU coupling reagent and NovaPEG Rink Amide resin were purchased from Novabiochem or Iris Biotech. Other reagents for peptide synthesis, solvents, buffers and metal salts were purchased from Sigma-Aldrich or Fluorochem. All buffer or metal solutions for spectroscopic measurements were prepared with ultrapure water produced by a Millipore Milli-Q purification system (purified to 18.2 MΩ.cm). Analytical HPLC/LRMS analyses were performed on an Agilent Infinity 1260 II system equipped with a 6125 MS (ESI) detector using a Waters XBridge BEH130 C18 (2.5 µm, 75 mm × 4.6 mm). Preparative HPLC separations were performed on a VWR LaPrepΣ system using

Waters XBridge Peptide BEH130 C18 (5 µm, 150 mm × 19 mm) or Waters XBridge Peptide BEH130 C18 (5 µm, 150 mm × 10 mm) columns at flow rates of 14 or 6 mL/min, respectively. Mobile phase consisted in a gradient of solvent A (0.1 % TFA in H_2O) and B (0.1 % TFA in MeCN/H_2O 9:1). For analytical separations, Method B consisted in 5% B during 1 min followed by a 5 to 100 % B gradient in 13 min at 1 mL/min. Eluate was monitored by electronic absorption at 214, 280 and 331 nm as well as by LRMS (ESI+) detection. ^{1}H, ^{13}C and DEPT NMR spectra were recorded at 400 MHz on a Varian Avance III 400 spectrometer at 298 K unless specified. All chemical shifts for ^{1}H and ^{13}C spectra were referenced to the residual solvent peak ($CDCl_3$ δ_H = 7.26 ppm and δ_C = 77.2 ppm). The following abbreviations were for peak multiplicities: s (singlet), d (doublet), t (triplet), q (quartet), dd (doublet of doublet), m (multiplet), br (broad peak(s)). LRMS(ESI) analyses were performed on a Thermo Scientific LXQ spectrometer. HRMS (ESI) were performed on a Thermo Scientific LTQ Orbitrap XL spectrometer or on a Waters Xevo G2-S QTof spectrometer with electrospray ionization.

Compound 2. CuI (12 mg, 63 µmol) and *tetrakis*(triphenylphosphine)palladium(0) (72 mg, 63 µmol) were dissolved in degassed TEA 12.5 mL). Then, a degassed solution of 9-(4-bromophenyl)-9H-carbazole (403 mg, 1.25 mmol) in THF (2.5 mL) was added followed by ethynyltrimethylsilane (230 µL, 1.6 mmol). The reaction mixture was stirred at 60 °C under argon for 24 h. The suspension was cooled to room temperature and filtered. The filtrate was evaporated under reduced pressure and AcOEt was added. The organic solution was washed with saturated NH_4Cl, water and saturated NH_4Cl. The organic phase was dried over Na_2SO_4 and the solvent was removed under reduced pressure to give a brown oily residue that was purified by flash chromatography (SiO_2, cyclohexane then cyclohexane/DCM 95/5) to give compound **2** (230 mg, 54 %). ^{1}H NMR (400 MHz, $CDCl_3$): δ = 8.15 (d, *J* = 7.8 Hz, 2H), 7.70 (d, *J* = 8.5 Hz, 2H), 7.53 (d, *J* = 8.5 Hz, 2H), 7.44-7.40 (m, 4H), 7.3'-7.28 (m, 2H), 0.31 (s, 9H) ppm. Spectroscopic data corresponded to literature.[60]

L-CC-Ar-Cz(tBu$_3$). Compound **2** (68 mg, 0.20 mmol), compound **1**[37] (158 mg, 0.200 mmol), were dissolved in a degassed mixture of DMF (16 mL) and TEA (0.65 mL). TBAF 1M in THF (200 µL, 200 µmol) and *bis*(triphenylphosphine)palladium(II) dichloride (14 mg, 20 µmol) were added to the solution and the mixture was stirred overnight at 90 °C. The solvents were removed under reduced pressure. The oily residue was dissolved in AcOEt. The organic solution was washed with saturated $NaHCO_3$ (3×) and dried over Na_2SO_4. The solvent was removed under reduced pressure. The oily residue was dissolved in EtOH (20 mL), then NaOH 3 M (1.4 mL) was added dropwise and the mixture was stirred for 15 min at room temperature. The suspension was centrifugated and the supernatant was neutralized with HCl 6 M. A precipitate was formed, which was eliminated by centrifugation. The solvents were removed under reduced pressure and the oily residue was dissolved in AcOEt. The organic solution was washed with saturated $NaHCO_3$ and dried over Na_2SO_4. The solvent was removed under reduced pressure to give a solid that was purified by HPLC. After freeze drying, a solid was obtained (144 mg, 57 % % calculated based of the formula **L-CC-Ar-Cz(tBu)$_3$·3TFA**). HPLC (anal.): t_R = 13.8 min (method B); ^{1}H NMR (400 MHz, $CDCl_3$): δ = 8.24 (s, 1H), 8.12 (d, *J* = 7.8 Hz, 2H), 7.77 (d, *J* = 8.3 Hz, 2H), 7.68 (s, 1H), 7.60 (d, *J* = 8.3 Hz, 2H), 7.46-7.36 (m, 4H), 7.32-7.26 (m, 2H), 4.49 (s, 2H), 3.84 (s, 2H), 3.7 – 3.0 (br, 20H), 1.45 (s, 9H), 1.41 (s, 18H) ppm; $^{13}C\{^{1}H\}$ NMR (100 MHz, $CDCl_3$): δ = 168.6, 165.8, 161.2 (q, *J* = 37 Hz, TFA), 149.1, 140.4, 139.2, 134.3, 133.8, 128.6, 127.0, 126.3, 123.8, 120.6, 120.3, 116.5 (q, *J* = 291 Hz, TFA), 109.8, 95.8, 86.5, 83.9, 83.4, 57.6, 55.4, 54.9, 51.0, 49.8, 28.1 ppm; LRMS (ESI+): monoisotopic *m/z* = 915.5 (+) (calculated *m/z* = 915.50 $[M+Na]^+$ for M = $C_{53}H_{66}N_6O_8$); HRMS (ESI+): monoisotopic *m/z* = 915.5014 (+) (calculated *m/z* = 915.5915 $[M+H]^+$ for M = $C_{53}H_{66}N_6O_8$).

L-Ar-Cz(tBu$_3$). Compound **1**[37] (200 mg, 0.250 mmol), 9-(4-(4,4,5,5-tetramethyl-1,3,2-dioxaborolan-2-yl)phenyl)-9H-carbazole (112 mg, 0.30 mmol), cesium fluoride (137 mg, 0.90 mmol) and *tetrakis*(triphenylphosphine)palladium(0) (polymer-bound, 62 mg, 0.025 mmol) were dissolved in anhydrous DMF (5 mL). The reaction was stirred at 90 °C under argon for 17 h. The mixture was filtered over celite and the solvent was removed under reduce pressure. AcOEt was added and the solution was washed with saturated $NaHCO_3$ (twice), brine (twice) and water. The organic layer was dried over Na_2SO_4 and the solvent was

removed under reduced pressure. The crude product was dissolved in EtOH (20 mL), then NaOH 6 M (4 mL) was added dropwise and the mixture was stirred for 10 min at room temperature. The solution was neutralized with HCl 6 M. A precipitate was formed. The solution was centrifugated, the supernatant was diluted in AcOEt and the organic solution was washed with brine then water and dried over Na_2SO_4. The solvent was removed under reduced pressure. The residue was dissolved in MeCN/H_2O 9:1 (v/v) containing 0.1% TFA (10 mL) and H_2O containing 0.1% TFA was added. A precipitate was formed. The supernatant was lyophilized and the obtained solid could be used without further purification (170 mg, 55% calculated based of the formula **L-Ar-Cz(tBu)$_3$·3TFA**). A small quantity was purified by HPLC for NMR characterization. HPLC (anal.): t_R = 13.2 min (method B); ^{1}H NMR (400 MHz, $CDCl_3$): δ = 8.45 (s, 1H), 8.12 (d, J = 7.7 Hz, 2H), 7.99 (s, 1H), 7.92 (d, J = 8.3 Hz, 2H), 7.72 (d, J = 8.3 Hz, 2H), 7.46-7.36 (m, 4H), 7.31 (ddd, J = 1.3, 7.3, 8.5 Hz, 2H), 4.63 (s, 2H), 3.90 (s, 2H), 3.8 – 2.8 (br, 20H), 1.44 (s, 9H), 1.36 (s, 18H) ppm; ^{13}C{^{1}H} NMR (100 MHz, $CDCl_3$): δ = 168.9, 165.9, 161.1 (q, J = 37 Hz, TFA), 150.5, 149.1, 140.4, 139.6, 134.9, 128.8, 127.5, 126.2, 125.1, 123.7, 122.6, 120.5, 116.4 (q, J = 291 Hz, TFA), 109.7, 84.2, 83.2, 57.6, 55.2, 54.6, 51.0, 50.7, 49.5, 49.2, 27.9 ppm; LRMS (ESI+): monoisotopic *m/z* = 913.6 (+) (calculated *m/z* = 913.5 $[M+Na]^+$ for M = $C_{51}H_{66}N_6O_8$); HRMS (ESI+): monoisotopic *m/z* = 891.5021 (+) (calculated *m/z* = 891.5015 $[M+H]^+$ for M = $C_{51}H_{66}N_6O_8$).

Peptide sequences. mTAT[L-Ar-Cz]: Ac-K(L-Ar-Cz)RKKRRQRRRG-NH_2; **mTAT[Ln·L-Ar-Cz] (Ln = Eu or Gd):** Ac-K(Ln·L-Ar-Cz)RKKRRQRRRG-NH_2; **mTAT[L-CC-Ar-Cz]:** Ac-K(L-CC-Ar-Cz)RKKRRQRRRG-NH_2; **mTAT[Ln·L-CC-Ar-Cz] (Ln = Eu or Gd):** Ac-K(Ln·L-CC-Ar-Cz)RKKRRQRRRG-NH_2; **CTAT[L-Ar-Cz]:** CK(L-Ar-Cz)RKKRRQRRRG-NH_2; **dTAT[Eu·L-Ar-Cz]:** **(**CK(Eu·L-Ar-Cz)RKKRRQRRRG-NH_2)$_2$ (disulfide bridge); **ZF5.3[L-Ar-Cz]:** Ac-K(L-Ar-Cz)AFSCNVCGKAFVLSRHLNRHLRVHRRAT-NH_2; **ZF5.3[Eu·L-Ar-Cz]:** Ac-K(Eu·L-Ar-Cz)AFSCNVCGKAFVLSRHLNRHLRVHRRAT-NH_2; **dFFLIPTAT:** **(**CFFLIPRKKRRQRRRG-NH_2)$_2$ (disulfide bridge).

Peptide synthesis. mTAT[Ln·L] conjugates, **dTAT[Eu·L-Ar-Cz]** and **ZF5.3[Eu·L-Ar-Cz]** were synthesized following previously described procedures.[37] **mTAT[L-Ar-Cz]:** HPLC (anal.): t_R = 8.4 min (method B); LRMS (ESI+): average *m/z* = 1136.4 (2+), 758.0 (3+), 568.9 (4+), 455.3 (5+), 379.7 (6+) / calculated av. *m/z* = 1136.33 $[M+2H]^{2+}$, 757.89 $[M+3H]^{3+}$, 568.67 $[M+4H]^{4+}$, 455.14 $[M+5H]^{5+}$, 379.44 $[M+6H]^{6+}$ for M = $C_{102}H_{164}N_{40}O_{20}$); deconvoluted mass found = 2271.5 / expected mass = 2270.65 (average isotopic composition). **CTAT[L-Ar-Cz]:** HPLC (anal.): t_R = 8.3 min (method B); LRMS (ESI+): average *m/z* = 778.3 (3+), 584.1 (4+), 467.5 (5+), 389.8 (6+) / calculated av. *m/z* = 778.26 $[M+3H]^{3+}$, 583.95 $[M+4H]^{4+}$, 467.56 $[M+5H]^{5+}$, 389.63 $[M+6H]^{6+}$ for M = $C_{103}H_{167}N_{41}O_{20}S$); deconvoluted mass found = 2332.0 / expected mass = 2331.75 (average isotopic composition). **ZF5.3[L-Ar-Cz]:** HPLC (anal.): t_R = 9.2 min (method B); LRMS (ESI+): average *m/z* = 1375.5 (3+), 1032.1 (4+), 825.9 (5+), 688.5 (6+), 590.3 (7+) / calculated av. *m/z* = 1375.60 $[M+3H]^{3+}$, 1031.95 $[M+4H]^{4+}$, 825.76 $[M+5H]^{5+}$, 688.30 $[M+6H]^{6+}$, 590.12 $[M+7H]^{7+}$ for M = $C_{187}H_{285}N_{61}O_{42}S_2$); deconvoluted mass found = 4124.0 / expected mass = 4123.78 (average isotopic composition). **mTAT[L-CC-Ar-Cz]:** HPLC (anal.): t_R = 6.0 min (method B); LRMS (ESI+): average *m/z* = 766.9 (3+), 575.0 (4+), 460.3 (5+) / calculated av. *m/z* = 765.90 $[M+3H]^{3+}$, 574.67 $[M+4H]^{4+}$, 459.94 $[M+5H]^{5+}$for M = $C_{104}H_{164}N_{40}O_{20}$); deconvoluted mass found = 2295.9 / expected mass = 2294.67 (average isotopic composition). **mTAT[Eu·L-Ar-Cz]:** HPLC (anal.): t_R = 8.5 min (method B); LRMS (ESI+): average *m/z* = 807.8 (3+), 606.2 (4+), 485.2 (5+), 404.5 (6+) / calculated av. *m/z* = 807.54 $[M+3H]^{3+}$, 605.91 $[M+4H]^{4+}$, 484.93 $[M+5H]^{5+}$, 404.27 $[M+6H]^{6+}$ for M = $C_{102}H_{161}N_{40}O_{20}Eu$); deconvoluted mass found = 2421.2 / expected mass = 2419.59 (average isotopic composition). **mTAT[Gd·L-Ar-Cz]:** HPLC (anal.): t_R = 8.5 min (method B); LRMS (ESI+): average *m/z* = 809.5 (3+), 607.3 (4+), 486.3 (5+), 405.3 (6+) / calculated av. *m/z* = 809.30 $[M+3H]^{3+}$, 607.22 $[M+4H]^{4+}$, 485.98 $[M+5H]^{5+}$, 405.15 $[M+6H]^{6+}$ for M = $C_{102}H_{161}N_{40}O_{20}Gd$); deconvoluted mass found = 2426.4 / expected mass = 2424.88 (average isotopic composition). **mTAT[Eu·L-CC-Ar-Cz]:** HPLC (anal.): t_R = 9.1 min (method B); LRMS (ESI+): average *m/z* = 816.0 (3+), 612.3 (4+), 490.0 (5+), 408.6 (6+) / calculated av. *m/z* = 815.55 $[M+3H]^{3+}$, 611.91 $[M+4H]^{4+}$, 489.73

$[M+5H]^{5+}$, 408.27 $[M+6H]^{6+}$ for M = $C_{104}H_{161}N_{40}O_{20}Eu$); deconvoluted mass found = 2445.2 / expected mass = 2443.61 (average isotopic composition). **mTAT[Gd·L-CC-Ar-Cz]:** HPLC (anal.): t_R = 9.0 min (method B); LRMS (ESI+): average *m/z* = 817.5 (3+), 613.4 (4+), 491.1 (5+), 409.3 (6+) / calculated av. *m/z* = 817.30 $[M+3H]^{3+}$, 613.23 $[M+4H]^{4+}$, 490.79 $[M+5H]^{5+}$, 409.16 $[M+6H]^{6+}$ for M = $C_{104}H_{161}N_{40}O_{20}Gd$); deconvoluted mass found = 2449.2 / expected mass = 2448.90 (average isotopic composition). **dTAT[Eu·L-Ar-Cz]:** HPLC (anal.): t_R = 8.9 min (method B); LRMS (ESI+): average *m/z* = 827.8 (6+), 709.8 (7+), 621.3 (8+), 552.3 (9+), 497.2 (10+), / calculated av. *m/z* = 827.57 $[M+6H]^{6+}$, 709.49 $[M+7H]^{7+}$, 620.93 $[M+8H]^{8+}$, 552.05 $[M+9H]^{9+}$, 496.94 $[M+10H]^{10+}$ for M = $C_{206}H_{326}N_{82}O_{40}S_2Eu_2$); deconvoluted mass found = 4961.6 / expected mass = 4959.37 (average isotopic composition). **ZF5.3[Eu·L-Ar-Cz]:** HPLC (anal.): t_R = 9.1 min (method B); LRMS (ESI+): average *m/z* = 1069.4 (4+), 855.8 (5+), 713.3 (6+), 611.7 (7+) / calculated av. *m/z* = 1069.19 $[M+4H]^{4+}$, 855.55 $[M+5H]^{5+}$, 713.13 $[M+6H]^{6+}$, 611.39 $[M+7H]^{7+}$ for M = $C_{187}H_{283}N_{61}O_{42}S_2Eu$); deconvoluted mass found = 4273.8 / expected mass = 4272.71 (average isotopic composition).

Electronic absorption. UV-Vis absorption spectra were recorded on a on a Varian Cary 50 spectrometer equipped with a thermo-regulated cell holder. Molar absorption coefficients were determined by titrating a solution of **mTAT[L-CC-Ar-Cz]** or **mTAT[L-Ar-Cz]** in HEPES buffer (10 mM, pH 7.5) by a solution of $EuCl_3$ (1.1 mM or 4.4 mM). These titrations are shown in Figure S4 of the Supporting Information.

Luminescence. Luminescence spectra were measured on a Varian Cary Eclipse spectrometer equipped with a thermo-regulated cell holder or on a modular Fluorolog FL3-22 spectrometer from Horiba-Jobin Yvon-Spex equipped with a double-grating excitation monochromator and an iHR320 imaging spectrometer coupled to Hamamatsu R928P and Hamamatsu R5509 photomultipliers for visible and NIR detection, respectively. Emission spectra were corrected for wavelength-dependent detector response. Time-gated Ln^{3+} luminescence spectra were acquired with 100 µs time delay and 2 ms gate time on the Varian Cary Eclipse spectrometer. Ln^{3+} luminescence lifetimes were measured using the Varian Cary Eclipse spectrometer and decay curves were fitted to a mono-exponential decay or a bi-exponential decay when required. Examples are given in Figure S5 of the Supporting Information. Quantum yields were determined using a Fluorolog FL3-22 spectrophotometer by a relative method with quinine sulphate in 0.5 M H_2SO_4 as a reference compound (Φ = 0.545)[61,62] using solutions of various concentrations having absorption below 0.1 at the excitation wavelength. The excitation wavelength was the same for the sample compound (S) and the reference. To determine the quantum yields of the sample compound, the following equation was used:

$$\Phi_S = \frac{A_S}{I_S} \times \frac{I_{ref}}{A_{ref}} \times \frac{{n_S}^2}{{n_{ref}}^2} \times \Phi_{ref} \quad (1)$$

where *A* is the absorbance at the excitation wavelength, *I* the integrated emission intensity and *n* the refractive index of the solvent. Estimated experimental error for the quantum yield determination is ~10 %. Refractive index values of dioxane/water and acetonitrile/water mixtures, were taken from the literature.[63,64] Values of viscosity (η) and polarity ($E_T(30)$) used to plot Figure 6 were taken from the literature.[65,66,63,67–69,49] Two-photon cross sections were determined as previously described.[37]

Cell culture, MTT proliferation assays and 2P microscopy. They were performed on HeLa cells as previously described.[37]

Acknowledgements

Authors acknowledge the Labex ARCANE, CBH-EUR-GS (ANR-17-EURE-0003), the Agence Nationale de la Recherche (ANR-18-CE06-0022 and ANR-21-CE29-0018) and the CEA FOCUS Biomarqueurs program for financial support. Imaging experiments were done on Microcell core facility of the Institute for Advanced Biosciences (UGA - Inserm U1209 - CNRS 5309). This facility belongs to the IBISA-ISdV platform, member of

the national infrastructure France-BioImaging supported by the French National Research Agency (ANR-10-INBS-04).

Supporting information available

HPLC chromatograms and LRMS spectra of **mTAT[L-Ar-Cz]**, **mTAT[Eu·L-Ar-Cz]** and **mTAT[Gd·L-Ar-Cz]**; absorbance spectrum of 9-(4-bromophenyl)-*9H*-carbazole; titrations for ε determination; Eu^{3+} luminescence decays of **mTAT[Eu·L-Ar-Cz]** and **mTAT[Eu·L-CC-Ar-Cz]**; 77 K phosphorescence emission spectra; absorption and luminescence spectra in DMF; absorption spectra of **dTAT[Eu·L-Ar-Cz]**; absorption and emission spectra of **ZF5.3[Eu·L-Ar-Cz]** (± Zn); protocols for the synthesis of model compounds for electrochemical measurements; electrochemical analysis of model compounds; 3D structure of ZF5.3; 2PM images of HeLa cells incubated with **dTAT[Eu·L-Ar-Cz]** at a toxic concentration; MTT assay for dFFLIPTAT and 2PM images (zoom) of HeLa cells incubated with **mTAT[Eu·L-Ar-Cz]** at 2.5 µM (PDF).

References

(1) Eliseeva, S. V.; Bünzli, J.-C. G. Lanthanide Luminescence for Functional Materials and Bio-Sciences. *Chem. Soc. Rev.* **2010**, *39* (1), 189–227. https://doi.org/10.1039/b905604c.
(2) Bünzli, J.-C. G. Lanthanide Luminescence for Biomedical Analyses and Imaging. *Chem. Rev.* **2010**, *110* (5), 2729–2755. https://doi.org/10.1021/cr900362e.
(3) Bünzli, J.-C. G. Lanthanide Light for Biology and Medical Diagnosis. *J. Lumin.* **2016**, *170*, 866–878. https://doi.org/10.1016/j.jlumin.2015.07.033.
(4) Pandya, S.; Yu, J.; Parker, D. Engineering Emissive Europium and Terbium Complexes for Molecular Imaging and Sensing. *Dalton Trans.* **2006**, No. 23, 2757–2766. https://doi.org/10.1039/B514637B.
(5) Montgomery, C. P.; Murray, B. S.; New, E. J.; Pal, R.; Parker, D. Cell-Penetrating Metal Complex Optical Probes: Targeted and Responsive Systems Based on Lanthanide Luminescence. *Acc. Chem. Res.* **2009**, *42* (7), 925–937. https://doi.org/10.1021/ar800174z.
(6) Amoroso, A. J.; Pope, S. J. A. Using Lanthanide Ions in Molecular Bioimaging. *Chem. Soc. Rev.* **2015**, *44* (14), 4723–4742. https://doi.org/10.1039/c4cs00293h.
(7) Sy, M.; Nonat, A.; Hildebrandt, N.; Charbonnière, L. J. Lanthanide-Based Luminescence Biolabelling. *Chem. Commun.* **2016**, *52* (29), 5080–5095. https://doi.org/10.1039/C6CC00922K.
(8) Jin, G.-Q.; Ning, Y.; Geng, J.-X.; Jiang, Z.-F.; Wang, Y.; Zhang, J.-L. Joining the Journey to near Infrared (NIR) Imaging: The Emerging Role of Lanthanides in the Designing of Molecular Probes. *Inorg. Chem. Front.* **2020**, *7* (2), 289–299. https://doi.org/10.1039/C9QI01132C.
(9) Zwier, J. M.; Bazin, H.; Lamarque, L.; Mathis, G. Luminescent Lanthanide Cryptates: From the Bench to the Bedside. *Inorg. Chem.* **2014**, *53* (4), 1854–1866. https://doi.org/10.1021/ic402234k.
(10) Mathieu, E.; Sipos, A.; Demeyere, E.; Phipps, D.; Sakaveli, D.; Borbas, K. E. Lanthanide-Based Tools for the Investigation of Cellular Environments. *Chem. Commun.* **2018**, *54* (72), 10021–10035. https://doi.org/10.1039/C8CC05271A.
(11) Bünzli, J.-C. G.; Eliseeva, S. V. Basics of Lanthanide Photophysics. In *Lanthanide Luminescence*; Hänninen, P., Härmä, H., Eds.; Springer Series on Fluorescence; Springer Berlin Heidelberg, 2011; pp 1–45.
(12) Rajendran, M.; Miller, L. W. Evaluating the Performance of Time-Gated Live-Cell Microscopy with Lanthanide Probes. *Biophys. J.* **2015**, *109* (2), 240–248. https://doi.org/10.1016/j.bpj.2015.06.028.
(13) Weissman, S. I. Intramolecular Energy Transfer: The Fluorescence of Complexes of Europium. *J. Chem. Phys.* **1942**, *10* (4), 214–217. https://doi.org/10.1063/1.1723709.
(14) Denk, W.; Strickler, J. H.; Webb, W. W. Two-Photon Laser Scanning Fluorescence Microscopy. *Science* **1990**, *248* (4951), 73–76. https://doi.org/10.1126/science.2321027.
(15) D'Aléo, A.; Picot, A.; Baldeck, P. L.; Andraud, C.; Maury, O. Design of Dipicolinic Acid Ligands for the Two-Photon Sensitized Luminescence of Europium Complexes with Optimized Cross-Sections. *Inorg. Chem.* **2008**, *47* (22), 10269–10279. https://doi.org/10.1021/ic8012975.
(16) Picot, A.; D'Aleo, A.; Baldeck, P. L.; Grichine, A.; Duperray, A.; Andraud, C.; Maury, O. Long-Lived Two-Photon Excited Luminescence of Water-Soluble Europium Complex: Applications in Biological Imaging Using Two-Photon Scanning Microscopy. *J. Am. Chem. Soc.* **2008**, *130* (5), 1532–1533.

https://doi.org/10.1021/ja076837c.
(17) D'Aléo, A.; Bourdolle, A.; Brustlein, S.; Fauquier, T.; Grichine, A.; Duperray, A.; Baldeck, P. L.; Andraud, C.; Brasselet, S.; Maury, O. Ytterbium-Based Bioprobes for Near-Infrared Two-Photon Scanning Laser Microscopy Imaging. *Angew. Chem., Int. Ed.* **2012**, *51* (27), 6622–6625. https://doi.org/10.1002/anie.201202212.
(18) Pålsson, L.-O.; Pal, R.; Murray, B. S.; Parker, D.; Beeby, A. Two-Photon Absorption and Photoluminescence of Europium Based Emissive Probes for Bioactive Systems. *Dalton Trans.* **2007**, No. 48, 5726–5734. https://doi.org/10.1039/B710717J.
(19) Kielar, F.; Congreve, A.; Law, G.; New, E. J.; Parker, D.; Wong, K.-L.; Castreño, P.; de Mendoza, J. Two-Photon Microscopy Study of the Intracellular Compartmentalisation of Emissive Terbium Complexes and Their Oligo-Arginine and Oligo-Guanidinium Conjugates. *Chem. Commun.* **2008**, No. 21, 2435–2437. https://doi.org/10.1039/B803864C.
(20) Soulié, M.; Latzko, F.; Bourrier, E.; Placide, V.; Butler, S. J.; Pal, R.; Walton, J. W.; Baldeck, P. L.; Le Guennic, B.; Andraud, C.; Zwier, J. M.; Lamarque, L.; Parker, D.; Maury, O. Comparative Analysis of Conjugated Alkynyl Chromophore–Triazacyclononane Ligands for Sensitized Emission of Europium and Terbium. *Chem.-Eur. J.* **2014**, *20* (28), 8636–8646. https://doi.org/10.1002/chem.201402415.
(21) Law, G.-L.; Wong, K.-L.; Man, C. W.-Y.; Tsao, S.-W.; Wong, W.-T. A Two-Photon Europium Complex as Specific Endoplasmic Reticulum Probe. *J. Biophotonics* **2009**, *2* (12), 718–724. https://doi.org/10.1002/jbio.200910052.
(22) Placide, V.; Pitrat, D.; Grichine, A.; Duperray, A.; Andraud, C.; Maury, O. Design and Synthesis of Europium Luminescent Bio-Probes Featuring Sulfobetaine Moieties. *Tetrahedron Lett.* **2014**, *55* (7), 1357–1361. https://doi.org/10.1016/j.tetlet.2014.01.025.
(23) Bui, A. T.; Grichine, A.; Brasselet, S.; Duperray, A.; Andraud, C.; Maury, O. Unexpected Efficiency of a Luminescent Samarium(III) Complex for Combined Visible and Near-Infrared Biphotonic Microscopy. *Chem.-Eur. J.* **2015**, *21* (49), 17757–17761. https://doi.org/10.1002/chem.201503711.
(24) Bui, A. T.; Roux, A.; Grichine, A.; Duperray, A.; Andraud, C.; Maury, O. Twisted Charge-Transfer Antennae for Ultra-Bright Terbium(III) and Dysprosium(III) Bioprobes. *Chem.-Eur. J.* **2018**, *24* (14), 3408–3412. https://doi.org/10.1002/chem.201705933.
(25) Bui, A. T.; Beyler, M.; Liao, Y.-Y.; Grichine, A.; Duperray, A.; Mulatier, J.-C.; Guennic, B. L.; Andraud, C.; Maury, O.; Tripier, R. Cationic Two-Photon Lanthanide Bioprobes Able to Accumulate in Live Cells. *Inorg. Chem.* **2016**, *55* (14), 7020–7025. https://doi.org/10.1021/acs.inorgchem.6b00891.
(26) Hamon, N.; Roux, A.; Beyler, M.; Mulatier, J.-C.; Andraud, C.; Nguyen, C.; Maynadier, M.; Bettache, N.; Duperray, A.; Grichine, A.; Brasselet, S.; Gary-Bobo, M.; Maury, O.; Tripier, R. Pyclen-Based Ln(III) Complexes as Highly Luminescent Bioprobes for In Vitro and In Vivo One- and Two-Photon Bioimaging Applications. *J. Am. Chem. Soc.* **2020**, *142* (22), 10184–10197. https://doi.org/10.1021/jacs.0c03496.
(27) Butler, S. J.; Lamarque, L.; Pal, R.; Parker, D. EuroTracker Dyes: Highly Emissive Europium Complexes as Alternative Organelle Stains for Live Cell Imaging. *Chem. Sci.* **2014**, *5* (5), 1750–1756. https://doi.org/10.1039/C3SC53056F.
(28) New, E. J.; Congreve, A.; Parker, D. Definition of the Uptake Mechanism and Sub-Cellular Localisation Profile of Emissive Lanthanide Complexes as Cellular Optical Probes. *Chem. Sci.* **2010**, *1* (1), 111–118. https://doi.org/10.1039/c0sc00105h.
(29) Rajapakse, H. E.; Reddy, D. R.; Mohandessi, S.; Butlin, N. G.; Miller, L. W. Luminescent Terbium Protein Labels for Time-Resolved Microscopy and Screening. *Angew. Chem., Int. Ed.* **2009**, *48* (27), 4990–4992. https://doi.org/10.1002/anie.200900858.
(30) Rajapakse, H. E.; Gahlaut, N.; Mohandessi, S.; Yu, D.; Turner, J. R.; Miller, L. W. Time-Resolved Luminescence Resonance Energy Transfer Imaging of Protein-Protein Interactions in Living Cells. *Proc. Natl. Acad. Sci. U. S. A.* **2010**, *107* (31), 13582–13587. https://doi.org/10.1073/pnas.1002025107.
(31) Mohandessi, S.; Rajendran, M.; Magda, D.; Miller, L. W. Cell-Penetrating Peptides as Delivery Vehicles for a Protein-Targeted Terbium Complex. *Chem.-Eur. J.* **2012**, *18* (35), 10825–10829. https://doi.org/10.1002/chem.201201805.
(32) Rajendran, M.; Yapici, E.; Miller, L. W. Lanthanide-Based Imaging of Protein-Protein Interactions in Live Cells. *Inorg. Chem.* **2014**, *53* (4), 1839–1853. https://doi.org/10.1021/ic4018739.
(33) Zou, X.; Rajendran, M.; Magda, D.; Miller, L. W. Cytoplasmic Delivery and Selective, Multicomponent Labeling with Oligoarginine-Linked Protein Tags. *Bioconjugate Chem.* **2015**, *26* (3), 460–465. https://doi.org/10.1021/bc500550z.
(34) Chen, T.; Pham, H.; Mohamadi, A.; Miller, L. W. Single-Chain Lanthanide Luminescence Biosensors for Cell-Based Imaging and Screening of Protein-Protein Interactions. *iScience* **2020**, *23* (9), 101533. https://doi.org/10.1016/j.isci.2020.101533.
(35) Starck, M.; Fradgley, J. D.; Di Vita, S.; Mosely, J. A.; Pal, R.; Parker, D. Targeted Luminescent Europium Peptide Conjugates: Comparative Analysis Using Maleimide and Para-Nitropyridyl Linkages for Organelle

Staining. *Bioconjugate Chem.* **2020**, *31* (2), 229–240. https://doi.org/10.1021/acs.bioconjchem.9b00735.
(36) Choi, J.-H.; Fremy, G.; Charnay, T.; Fayad, N.; Pécaut, J.; Erbek, S.; Hildebrandt, N.; Martel-Frachet, V.; Grichine, A.; Sénèque, O. Luminescent Peptide/Lanthanide(III) Complex Conjugates with Push–Pull Antennas: Application to One- and Two-Photon Microscopy Imaging. *Inorg. Chem.* **2022**, *61* (50), 20674–20689. https://doi.org/10.1021/acs.inorgchem.2c03646.
(37) Malikidogo, K. P.; Charnay, T.; Ndiaye, D.; Choi, J.-H.; Bridou, L.; Chartier, B.; Erbek, S.; Micouin, G.; Banyasz, A.; Maury, O.; Martel-Frachet, V.; Grichine, A.; Sénèque, O. Efficient Cytosolic Delivery of Luminescent Lanthanide Bioprobes in Live Cells for Two-Photon Microscopy. *Chem. Sci.* **2024**, *15* (25), 9694–9702. https://doi.org/10.1039/D4SC00896K.
(38) Appelbaum, J. S.; LaRochelle, J. R.; Smith, B. A.; Balkin, D. M.; Holub, J. M.; Schepartz, A. Arginine Topology Controls Escape of Minimally Cationic Proteins from Early Endosomes to the Cytoplasm. *Chem. Biol.* **2012**, *19* (7), 819–830. https://doi.org/10.1016/j.chembiol.2012.05.022.
(39) LaRochelle, J. R.; Cobb, G. B.; Steinauer, A.; Rhoades, E.; Schepartz, A. Fluorescence Correlation Spectroscopy Reveals Highly Efficient Cytosolic Delivery of Certain Penta-Arg Proteins and Stapled Peptides. *J. Am. Chem. Soc.* **2015**, *137* (7), 2536–2541. https://doi.org/10.1021/ja510391n.
(40) D'Aléo, A.; Allali, M.; Picot, A.; Baldeck, P. L.; Toupet, L.; Andraud, C.; Maury, O. Sensitization of Eu(III) Luminescence by Donor-Phenylethynyl-Functionalized DTPA and DO3A Macrocycles. *C. R. Chim.* **2010**, *13* (6–7), 681–690. https://doi.org/10.1016/j.crci.2010.01.008.
(41) Regueiro-Figueroa, M.; Bensenane, B.; Ruscsak, E.; Esteban-Gomez, D.; Charbonniere, L. J.; Tircso, G.; Toth, I.; de Blas, A.; Rodriguez-Blas, T.; Platas-Iglesias, C. Lanthanide Dota-like Complexes Containing a Picolinate Pendant: Structural Entry for the Design of Ln(III)-Based Luminescent Probes. *Inorg. Chem.* **2011**, *50* (9), 4125–4141. https://doi.org/10.1021/ic2001915.
(42) Monteiro, J. H. S. K.; Fetto, N. R.; Tucker, M. J.; de Bettencourt-Dias, A. Luminescent Carbazole-Based EuIII and YbIII Complexes with a High Two-Photon Absorption Cross-Section Enable Viscosity Sensing in the Visible and Near IR with One- and Two-Photon Excitation. *Inorg. Chem.* **2020**, *59* (5), 3193–3199. https://doi.org/10.1021/acs.inorgchem.9b03561.
(43) Vivès, E.; Brodin, P.; Lebleu, B. A Truncated HIV-1 Tat Protein Basic Domain Rapidly Translocates through the Plasma Membrane and Accumulates in the Cell Nucleus. *J. Biol. Chem.* **1997**, *272* (25), 16010–16017. https://doi.org/10.1074/jbc.272.25.16010.
(44) Erazo-Oliveras, A.; Najjar, K.; Dayani, L.; Wang, T.-Y.; Johnson, G. A.; Pellois, J.-P. Protein Delivery into Live Cells by Incubation with an Endosomolytic Agent. *Nat. Methods* **2014**, *11* (8), 861–867. https://doi.org/10.1038/nmeth.2998.
(45) Beeby, A.; Clarkson, I. M.; Dickins, R. S.; Faulkner, S.; Parker, D.; Royle, L.; Sousa, A. S. de; Williams, J. A. G.; Woods, M. Non-Radiative Deactivation of the Excited States of Europium, Terbium and Ytterbium Complexes by Proximate Energy-Matched OH, NH and CH Oscillators: An Improved Luminescence Method for Establishing Solution Hydration States. *J. Chem. Soc., Perkin Trans. 2* **1999**, No. 3, 493–504. https://doi.org/10.1039/A808692C.
(46) Karon, K.; Lapkowski, M. Carbazole Electrochemistry: A Short Review. *J. Solid State Electrochem.* **2015**, *19* (9), 2601–2610. https://doi.org/10.1007/s10008-015-2973-x.
(47) Horrocks, W. D.; Bolender, J. P.; Smith, W. D.; Supkowski, R. M. Photosensitized near Infrared Luminescence of Ytterbium(III) in Proteins and Complexes Occurs via an Internal Redox Process. *J. Am. Chem. Soc.* **1997**, *119* (25), 5972–5973. https://doi.org/10.1021/ja964421l.
(48) Kovacs, D.; Mathieu, E.; Kiraev, S. R.; Wells, J. A. L.; Demeyere, E.; Sipos, A.; Borbas, K. E. Coordination Environment-Controlled Photoinduced Electron Transfer Quenching in Luminescent Europium Complexes. *J. Am. Chem. Soc.* **2020**, *142* (30), 13190–13200. https://doi.org/10.1021/jacs.0c05518.
(49) Reichardt, C. Solvatochromic Dyes as Solvent Polarity Indicators. *Chem. Rev.* **1994**, *94* (8), 2319–2358. https://doi.org/10.1021/cr00032a005.
(50) Weller, A. Electron-Transfer and Complex Formation in the Excited State. *Pure Appl. Chem.* **1968**, *16* (1), 115–124. https://doi.org/10.1351/pac196816010115.
(51) Beeby, A.; Faulkner, S.; Williams, J. A. G. pH Dependence of the Energy Transfer Mechanism in a Phenanthridine-Appended Ytterbium Complex. *J. Chem. Soc., Dalton Trans.* **2002**, No. 9, 1918–1922. https://doi.org/10.1039/B201867P.
(52) Kocsi, D.; Kovacs, D.; Wells, J. A. L.; Borbas, K. E. Reduced Quenching Effect of Pyridine Ligands in Highly Luminescent Ln(III) Complexes: The Role of Tertiary Amide Linkers. *Dalton Trans.* **2021**, *50* (45), 16670–16677. https://doi.org/10.1039/D1DT02893F.
(53) Parker, D.; D. Fradgley, J.; Delbianco, M.; Starck, M.; W. Walton, J.; M. Zwier, J. Comparative Analysis of Lanthanide Excited State Quenching by Electronic Energy and Electron Transfer Processes. *Faraday Discuss.* **2022**, *234* (0), 159–174. https://doi.org/10.1039/D1FD00059D.
(54) Parker, D. Luminescent Lanthanide Sensors for pH, *p*O2 and Selected Anions. *Coord. Chem. Rev.* **2000**,

205 (1), 109–130. https://doi.org/10.1016/S0010-8545(00)00241-1.
(55) Cao, R.; Wallrabe, H. K.; Periasamy, A. Multiphoton FLIM Imaging of NAD(P)H and FAD with One Excitation Wavelength. *J. Biomed. Opt.* **2020**, *25* (1), 014510. https://doi.org/10.1117/1.JBO.25.1.014510.
(56) Qin, Y.; Xia, Y. Simultaneous Two-Photon Fluorescence Microscopy of NADH and FAD Using Pixel-to-Pixel Wavelength-Switching. *Front. Phys.* **2021**, *9*, 642302. https://doi.org/10.3389/fphy.2021.642302.
(57) Klug, A. The Discovery of Zinc Fingers and Their Applications in Gene Regulation and Genome Manipulation. *Annu. Rev. Biochem.* **2010**, *79*, 213–231. https://doi.org/10.1146/annurev-biochem-010909-095056.
(58) Sénèque, O.; Latour, J.-M. Coordination Properties of Zinc Finger Peptides Revisited: Ligand Competition Studies Reveal Higher Affinities for Zinc and Cobalt. *J. Am. Chem. Soc.* **2010**, *132* (50), 17760–17774. https://doi.org/10.1021/ja104992h.
(59) Allen, J.; Pellois, J.-P. Hydrophobicity Is a Key Determinant in the Activity of Arginine-Rich Cell Penetrating Peptides. *Sci. Rep.* **2022**, *12* (1), 15981. https://doi.org/10.1038/s41598-022-20425-y.
(60) Hayashi, M.; Sakamoto, R.; Nishihara, H. Extremely Efficient and Reversible Visible-Light Photochromism and Accompanying Switch of Electronic Communication in N-Phenylcarbazole-Appended Diethynylethene. *Chem.-Eur. J.* **2012**, *18* (28), 8610–8613. https://doi.org/10.1002/chem.201200794.
(61) Brouwer, A. M. Standards for Photoluminescence Quantum Yield Measurements in Solution (IUPAC Technical Report). *Pure Appl. Chem.* **2011**, *83* (12), 2213–2228. https://doi.org/10.1351/PAC-REP-10-09-31.
(62) Resch-Genger, U.; Rurack, K. Determination of the Photoluminescence Quantum Yield of Dilute Dye Solutions (IUPAC Technical Report). *Pure Appl. Chem.* **2013**, *85* (10), 2005–2013. https://doi.org/10.1351/PAC-REP-12-03-03.
(63) Besbes, R.; Ouerfelli, N.; Latrous, H. Density, Dynamic Viscosity, and Derived Properties of Binary Mixtures of 1,4 Dioxane with Water at T = 298.15 K. *J. Mol. Liq.* **2009**, *145* (1), 1–4. https://doi.org/10.1016/j.molliq.2008.09.009.
(64) Schott, H. Densities, Refractive Indices, and Molar Refractions of the System Water-Dioxane at 25° C. *J. Chem. Eng. Data* **1961**, *6* (1), 19–20. https://doi.org/10.1021/je60009a006.
(65) Wode, H.; Seidel, W. Precise viscosity measurements of binary liquid mixtures of acetonitrile-water and 1,3-dimethyl-2-imidazolidinone-water. *Bunsenges. Phys. Chem.* **1994**, *98* (7), 927–934. https://doi.org/10.1002/bbpc.19940980706.
(66) El Seoud, O. A.; El Seoud, M. I.; Farah, J. P. S. Kinetics of the pH-Independent Hydrolysis of Bis(2,4-Dinitrophenyl) Carbonate in Acetonitrile−Water Mixtures: Effects of the Structure of the Solvent. *J. Org. Chem.* **1997**, *62* (17), 5928–5933. https://doi.org/10.1021/jo970070x.
(67) Sánchez, F. G.; Díaz, A. N.; Algarra, M.; Lovillo, J.; Aguilar, A. Time Resolved Spectroscopy of 2-(Dimethylamine)Fluorene. Solvent Effects and Photophysical Behavior. *Spectrochimica Acta Part A: Molecular and Biomolecular Spectroscopy* **2011**, *83* (1), 88–93. https://doi.org/10.1016/j.saa.2011.07.083.
(68) Spange, S. Polarity of Organic Solvent/Water Mixtures Measured with Reichardt's B30 and Related Solvatochromic Probes—A Critical Review. *Liquids* **2024**, *4* (1), 191–230. https://doi.org/10.3390/liquids4010010.
(69) Bernal-García, J. M.; Guzmán-López, A.; Cabrales-Torres, A.; Estrada-Baltazar, A.; Iglesias-Silva, G. A. Densities and Viscosities of (N,N-Dimethylformamide + Water) at Atmospheric Pressure from (283.15 to 353.15) K. *J. Chem. Eng. Data* **2008**, *53* (4), 1024–1027. https://doi.org/10.1021/je700671t.

Table of contents